Interconversion of δ and λ Forms of Six-Membered Chelate Cycles − A Quantitative NMR Spectroscopic Study of (Diphosphane)rhodium Compounds

Axel Frick,[a] Volker Schulz,[a] and Gottfried Huttner*[a]

Prof. Dr. Matthias Drieß in recognition of his outstanding contributions to inorganic chemistry

Keywords: Conformational analysis / Diphosphanes / Rhodium / Kinetics / Thermodynamics

The stereochemical flexibility of six-membered chelate cycles containing phosphorus donor groups has not yet been analysed in detail. With a number of compounds of the type $[\{\kappa\text{-}PR_2CH_2CH(OH)CH_2\text{-}\kappa\text{-}PR'_2\}Rh(\eta^4\text{-}COD)]^+PF_6^-$ at hand, and since the solid state structures and the catalytic properties of these compounds are known, an ideal opportunity to study this topic was available. After assigning all of the important ^1H, ^{13}C, and ^{31}P NMR spectroscopic resonances by a combination of one- and two-dimensional NMR spectroscopic methods quantitative interpretation of the 2D NOESY/EXSY spectra was achieved for four compounds [PR_2 = $PMes_2$; PR'_2 = PPh_2 (**1**), DBP (**2**), PEt_2 (**3**), P(*o*-anisyl)$_2$ (**4**)]. It is found that the conformations that these compounds adopt in solution are similar to the ones observed for them in the solid state. The conformational ensemble in solution comprises λ twist and δ twist forms; λ and δ isomers are clearly differentiated by quantitative NOE-based structure analysis (distance geometry). Since the sense of chirality of the ligand is known, an absolute assignment of these conformations is possible. The equilibrium constants at 298 K for the δ ⇄ λ isomerisation of compounds **1**–**4** are not very different from one another, with reaction enthalpies ranging from −8 to −2 kJ mol^{-1} and the reaction entropies in the range of −10 to 8 J K^{-1} mol^{-1}. The activation barriers are again similar for **1**–**4** and lie at $\Delta H^{\neq} \approx 64$ kJ mol^{-1}. It is observed that the mesityl entities at the $PMes_2$ donor groups behave as coupled rotors with two rotational pathways open to them during the δ ⇄ λ interconversion while they are rotationally fixed in the λ and δ conformations themselves. Comparing the above results with the enantioselective discrimination found for the same compounds in hydrogenation experiments it becomes clear that there is no direct correlation between the preference of one twist form over the other in the precatalyst and its chiral performance.

Introduction

Enantiopure chelate ligands play an important role in metal-mediated enantioselective catalyses. Amongst chelate ligands which contain a saturated carbon chain as a linker between the donor groups, the ones forming five-membered cycles have been found to be most effective.[1] These cycles have only one torsional degree of freedom as soon as three valence angles and five distances are defined, such that their conformational behaviour may easily be controlled, e.g. DIPAMP.[2,3] If larger chelate cycles have been found to be effective in enantioselective catalyses they almost inevitably contain unsaturated parts such that the number of independent coordinates of torsional freedom is still low due to the fixed conformation at the double bonds, e.g. BINAP.[4] In some other cases where the conformation of the chelate cycle is almost inflexible, by the nature of the covalent framework, enantiodiscrimination ensues from the chirality of substituent groups at the chelate cycle, e.g. PHOX.[5] It is not astonishing therefore that chelate ligands containing a saturated three-carbon chain as a linker between the donor groups have not been studied much as coligands in enantioselective catalyses. The six-membered cycles derived from them have an additional degree of torsional freedom with respect to five-membered cycles, once the six distances and four valence angles are defined.[6] Nevertheless, it has been found that six-membered diphosphane chelate cycles may be quite efficient in enantioselective catalyses.[7,8] Transfer of the chiral information from the chelate metal template to the substrates must then occur via the chirally induced preference of one of the chiral conformations of the chelate cycle over the others. If six-membered chelate cycles are generally found to be inefficient in enantioselective catalyses the reason for this might well be that the diastereoselection of one ring conformation over the others is less efficient in six-membered cycles as compared to the one in five-membered ones. Since quantitative information about the conformational enantiomerisation of phos-

[a] Anorganisch-Chemisches Institut der Universität Heidelberg, Im Neuenheimer Feld 270, 69120, Germany
Fax: (internat.) + 49-(0)6221/545707
E-mail: g.huttner@indi.aci.uni-heidelberg.de
Supporting information for this article is available on the WWW under http://www.eurjic.org or from the author.

phorus-containing six-membered chelate cycles is still missing, it appeared worthwhile to study such conformational enantiomerisation processes in more detail. In this paper we report on an NMR analysis of several compounds of the type $[\{\kappa\text{-}PR_2CH_2CH(OH)CH_2\text{-}\kappa\text{-}PR'_2\}Rh(\eta^4\text{-}COD)]^+PF_6^-$ which results in precise estimates of the thermodynamic and kinetic parameters which control the conformational inversion of their six-membered chelate cycles.

Results

The syntheses and catalytic properties of compounds **1**−**7** (Figure 1) are described in the literature.[8] The solid state structures of these compounds are well known with the exception of the structures of **3** and **7**.[8]

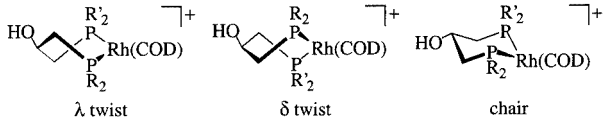

Compound	PR_2	PR'_2	X-ray		Chirality[b]
1	$PMes_2$	PPh_2	twist	λ,δ	(*S*)
2	DBP	$PMes_2$	twist	δ	(*R*)[c]
3	$PMes_2$	PEt_2	twist	λ,δ	(*S*,*R*)
4	$PMes_2$	P(2-MeOPh)$_2$	twist	λ,δ	(*R*)
5	P(2-MeOPh)$_2$	PPh_2	twist	λ,δ	(*S*)
6	PPh_2	P(*o*-Tol)$_2$	chair	OH-*eq*	(*R*)
7	P(*o*-Tol)$_2$	PEt_2	chair	OH-*eq*	(*S*,*R*)

Figure 1. Compounds **1**−**7**[a]
[a] The formulae indicate the constitution of compounds **1**−**7** as well as the three basic types of conformations (λ twist, δ twist, chair) which characterise the folding of the six-membered chelate cycle as found by X-ray analyses of crystals of the compounds. [b] The items in this column refer to the chirality of the ligand used for preparing the crystal material to which the X-ray data refer and from which the solutions for NMR spectroscopic analyses were prepared. [c] In the original paper[8] the sense of chirality of **2** was erroneously assigned as (*S*).

The structures of these latter two compounds have been determined for the racemates of compounds **3** and **7**.[9] The spread of substitution patterns in **1**−**7** and the fact that two conformational isomers are generally observed for these compounds in NMR studies[8] appeared to warrant a detailed NMR analysis of their conformational behaviour. Since, in addition, the solid state structures of the compounds are known, dissolving the crystals at low temperatures should produce solutions that contain the compounds in the same conformation as pertinent to the crystal. These conformations might well be metastable in solution at low temperatures and might thus help assign NMR signals to individual conformations. In the following paragraphs the procedures of complete assignment of all the relevant NMR signals of **1**−**4** will be described first (*Assignment of the NMR Spectra of **1**−**4***).

An EXSY analysis of the exchange processes between different ring conformations is described next (*Dynamic Exchange Processes*).

The information obtained by dissolving crystalline samples of **1**−**7** at low temperatures is given in the following paragraph (*Results from Dissolving Crystals of **1**−**7** at Low Temperatures*).

The last paragraph deals with the quantitative (distance geometry) NOE structure analysis of **1**−**4** (*Quantitative NMR Structure Analysis*).

Assignment of the NMR Spectra of 1−4

The general procedure of the assignment is given here for **1**. The procedures used for assigning the NMR resonances of **2**−**4** are, mutatis mutandis, the same. A view of the λ and δ conformations of **1** as found in the crystal[8] is shown in Figure 2.

The scheme adopted for referencing individual nuclei is shown in Figure 3.

The equilibrium between the λ and δ forms, that is observed in solution necessarily exchanges the positions that the substituents of the chelate ligand occupy with respect to the chelate cycle (Figure 4).

Thus, the mesityl group that is in a pseudo-axial position in the λ isomer (Figure 4, left) will be in a pseudo-equatorial position when the λ conformation transforms into the δ isomer. The same type of exchange occurs not only for the PR_2 groups, but also for the CH_2 protons of the chelate cycle (Figure 4). Referring to Figure 4 it is clear that the labelling scheme has been chosen, such as to identify the protons of the chelate cycle in the λ isomer by an unprimed number and refer to the same protons in the δ isomer by a primed number. The pseudo-axial or pseudo-equatorial position of these protons may always be extracted by inspecting Figure 4. If necessary, the atom identifier has been additionally labelled by the suffix *ax* or *eq* respectively.

A solution of **1** in CD_2Cl_2 contains two isomeric forms of **1** in a ratio of approximately 5:1, at 298 K. This had already been inferred from ^{31}P NMR spectroscopy.[8] The assignment of the individual nuclei of these two isomers is based on a combination of one- and two-dimensional NMR techniques including ^1H-^{31}P HMBC,[10] ^1H-^{13}C HSQC,[11] ^1H-^{13}C HMBC,[10] ^1H-^1H DQF-COSY,[12] and ^1H-^1H NOESY/EXSY.[13] DQF-COSY spectra at 298 K show the signals referring to the two isomers in an intensity ratio of 5:1 and allow one to clearly separate the data referring to one or the other isomer.

^1H-^{31}P HMBC spectra show that the mesityl groups are bonded to P1 (strong correlations to all of the protons of the mesityl groups). The protons H31,35 and H37,41 (Figure 3) are strongly correlated with P2 and must thus be the *ortho*-protons of the phenyl groups at the PPh_2 entity. Their correlations with the *meta*- and *para*-protons of the respective phenyl groups are evident from the COSY data (Table 3). The same type of correlation is found for the minor isomer.

The ^{13}C NMR signals of **1** were assigned by their ^1H-^{13}C correlations using ^1H-^{13}C HSQC and ^1H-^{13}C HMBC techniques. So far the assignment cannot differentiate be-

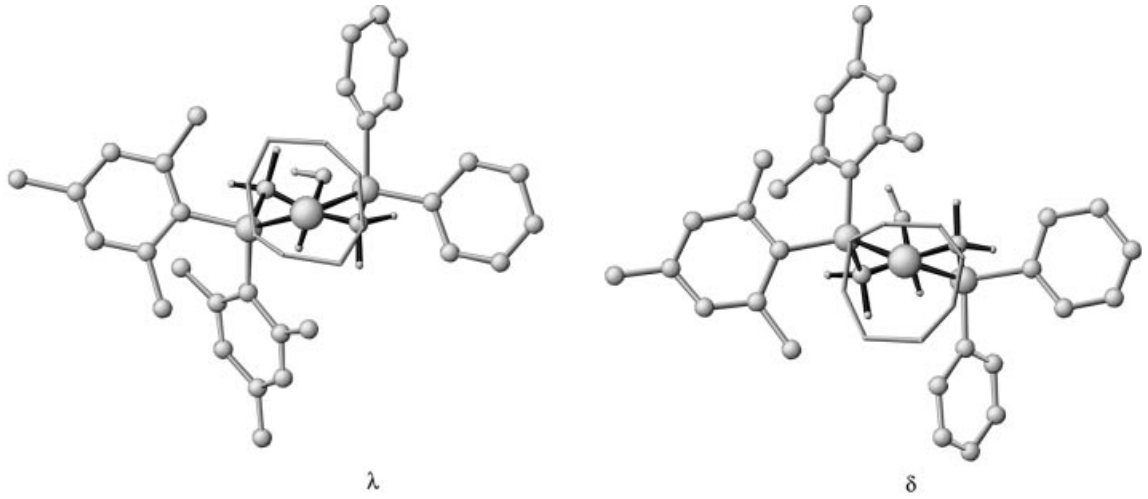

Figure 2. λ twist and δ twist isomers as found for independent constituents in the crystal of **1**; left-hand side: λ isomer; right-hand side: δ isomer; fFor the sake of clarity bonds to the carbon atoms of the COD ligands are not shown; hydrogen atoms are only shown for the chelate cycles

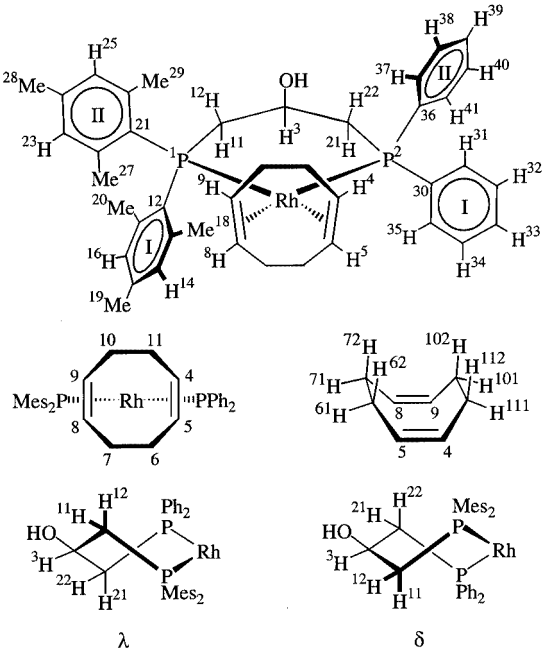

Figure 3. Labelling scheme used for **1**; the same numeric label as the hydrogen atoms to which they are bound, in general, designates the individual carbon atoms; carbon atoms belonging to the CH_2 groups of the COD ligand have labels which are numerically related to the labels used for the hydrogen atoms to which they are connected (e.g. C7−H71/H72, see figure); the carbon atoms of the three-carbon chain of the chelate ligand are numbered accordingly such that C1 binds to H11/H12, C2 to H21/H22, and C3 to H3; the labelling of the carbon atoms of the aryl groups is such that the carbon atoms have the same label as the respective protons; thus, C23 is bonded to H23, etc.; the carbon atoms are labelled with consecutive numbers around the cycles; the sense in which the numbers increase is evident from the labels assorted to the arene protons. The *ipso*-carbon atoms bonded to the phosphorus atoms have the lowest number in each case (C12, C21 for the mesityl groups; C30, C36 for the phenyl groups

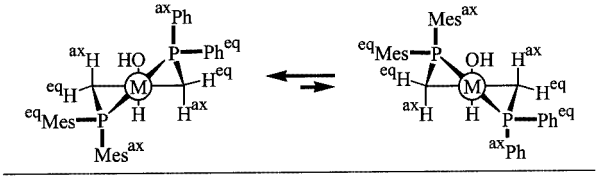

major isomer (λ)				minor isomer (δ)			
H^{eq}	H11	Mes^{eq}	H23–H29	H^{ax}	H11′	Mes^{ax}	H23′–H29′
H^{ax}	H12	Mes^{ax}	H14–H20	H^{eq}	H12′	Mes^{eq}	H14′–H20′
H^{eq}	H22	Ph^{eq}	H31–H35	H^{ax}	H22′	Ph^{ax}	H31′–H35′
H^{ax}	H21	Ph^{ax}	H37–H41	H^{eq}	H21′	Ph^{eq}	H37′–H41′

Figure 4. Labelling scheme for the two conformational isomers of **1**; the labelling scheme was chosen such that it refers to the identity of the specific atoms; this means that a proton that may occupy a pseudo-axial position in one isomer may find itself in a pseudo-equatorial position in the other one; the NMR spectroscopic signals referring to this specific proton will therefore find themselves at two distinctly different positions; throughout the paper the convention is adopted to assign unprimed numbers to the protons of the λ isomer and use primed numbers for the ones of the δ isomer. The pseudo-axial or pseudo-equatorial position of a proton, be it primed or unprimed, may be unequivocally inferred from the figure as given; for the ease of reading, the suffixes *ax* and *eq* are added to the labels wherever confusion might arise

tween e.g. nuclei in pseudo-axial and pseudo-equatorial groups, i.e. between different positions relative to the conformation of the chelate cycle. This differentiation is possible by NOE spectroscopy. Taking the λ and δ conformations observed for **1** in the crystal (Figure 2) as the ruler for distance based arguments the observed NOE cross-peaks can be consistently assigned.

The major isomer is found to correspond to the λ form of the chelate cycle (see below). The results are easily interpreted with respect to Figure 2 (left-hand side) which shows the structure of the λ isomer as found in the crystal. Referring to this figure the qualifiers left, right, top, and bottom make definite sense. The NOE analysis allows one to discriminate between the positions of individual groups with respect to these qualifiers. There are chains of contacts that link the top and bottom half of the molecule. A link on the rear side of the molecule (Figure 2, left) between the left-

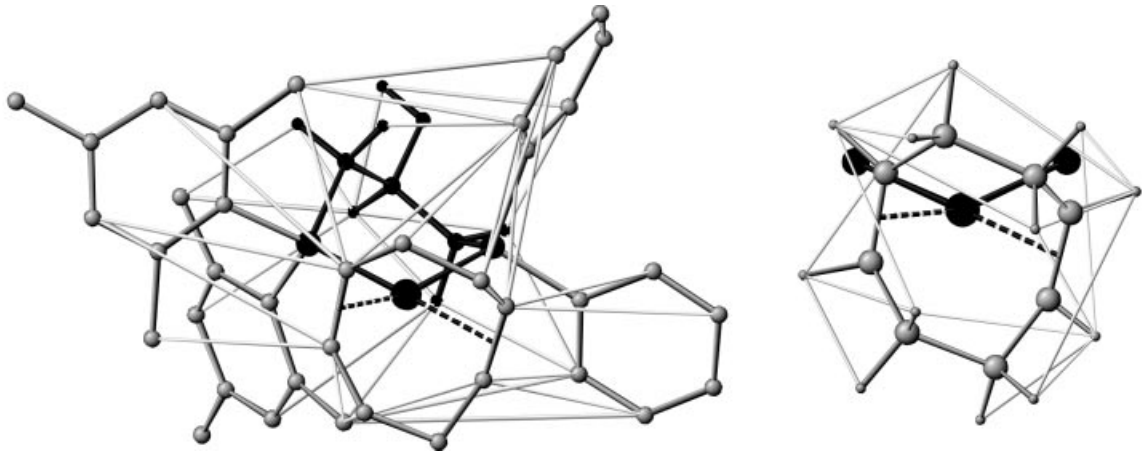

Figure 5. Scaffolding of NOE contacts characterising the λ twist conformer of **1**; NOE contacts are shown as light-grey shaded rods; right-hand side: conformationally relevant contacts within the COD coligand; left-hand side: contacts characterising the conformation of **1** as a whole (only a subset of observed contacts is shown; the full set is given in Table 8)

and the right-hand part of the molecule is formed by a number of contacts each of them involving the protons of the $CH_2-CH(OH)-CH_2$ linker (see above). On the front side of the molecule the left- and right-hand sides are also bridged by some interproton contacts (H18···H5, H18···H31,35; Figure 2 and 3). A tight scaffolding is therefore built up by the NOE contacts.

This scaffolding is shown in Figure 5 for the major isomer. The pertinent numeric information obtained by transforming NOE volume integrals into distances is given in Table 8. The NOE analysis of the minor isomer follows steps analogous to the ones used for the analysis of the major isomer. Due to the 1:5 ratio between the concentrations of the two isomers at the measuring temperature (298 K) a smaller number of contacts is observed. With the combination of methods described so far all the relevant ^1H-, ^{13}C-, and ^{31}P NMR signals of **1** can unequivocally be assigned (Table 3, 4, and 5). The details of the assignment of **1** are given in the Supporting Information.

Analogous procedures were used to assign individual nuclei in compounds **2**−**4**. The results pertaining to the assignment of **2**−**4** are shown in Table 5 and the Supporting Information.

Dynamic Exchange Processes

Dynamic exchange processes had already been found by variable-temperature 1D NMR spectroscopy for compounds of the type **1**−**7**.[8] To further elucidate these processes and to quantify activation barriers, 2D EXSY spectroscopy was applied to compounds **1**−**4**. Figure 6 shows parts of the 2D ^1H EXSY spectrum which characterises the dynamic exchange occurring for **1** in a CD_2Cl_2 solution at 298 K.

It is seen (Figure 6, left-hand side) that H3 exchanges with H3′; H11 is involved in a dynamic exchange process with H11′; H12 exchanges with H12′ and H22 is seen to exchange with H22′. It is clear from these observations that the shape of the chelate cycle switches between two conformations. With respect to the solid state structure of **1** which contains the λ and the δ isomers (Figure 2) the most

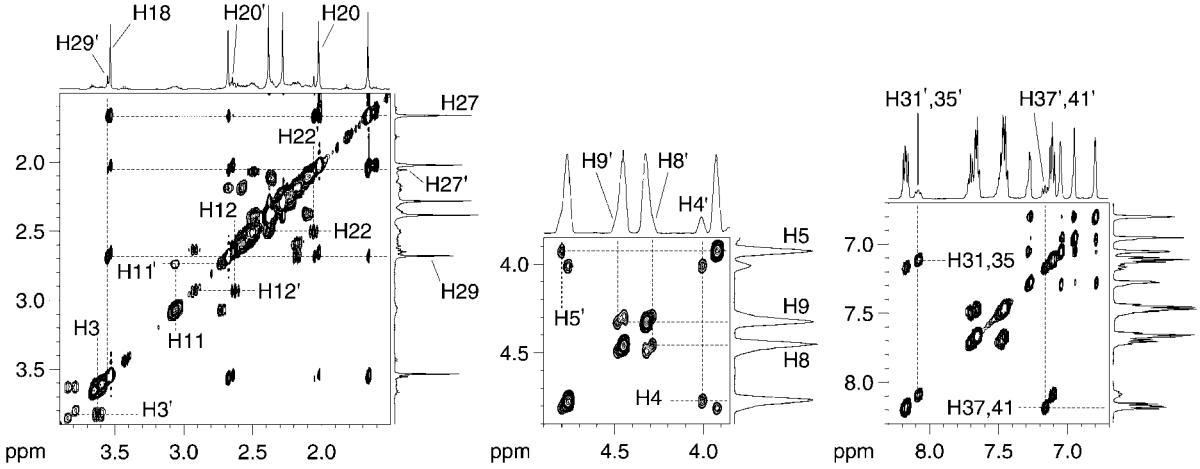

Figure 6. ^1H EXSY spectrum of **1** at 298 K; mixing time: 400 ms; all parts of the NOESY/EXSY spectrum of **1** are shown for which EXSY peaks can be observed; NOE peaks are suppressed in the figures shown

probable working hypothesis is to assume that the NMR observations pertain to the dynamic exchange between these two conformations (Figure 4). This hypothesis is proved by a series of further arguments including quantitative modelling of the conformations (see below). The part of the spectrum that characterises the dynamic behaviour of the COD coligand is shown in the center of Figure 6; H4 and H4′, as well as H5 and H5′, are in exchange with each other and so are H8/H8′ as well as H9/H9′. Exchange of the olefinic protons is hence only observed between protons at one and the same double bond. There is no cross-exchange between protons of the two different double bonds and any exchange process corresponding to a rotation of the COD coligand can therefore be ruled out. The observed process must then be due to an exchange of the surroundings of these olefinic protons such that, technically spoken, the COD coligand serves as a spectator ligand. Referring to Figure 2 it is seen that the position of the olefinic protons with respect to the PR_2 groups is just exchanged in the two isomers. In the course of the dynamic exchange between the two twist conformations (Figure 2) the substituents at the PR_2 groups must exchange their position with respect to their pseudo-axial or pseudo-equatorial positions. It is then expected that the phenyl *ortho*-protons H31,35 of one conformational isomer will exchange with the phenyl *ortho*-protons H31′,35′ of the other isomer (Figure 3 and 4). As Figure 6 (right-hand side) shows, this is in fact observed. The phenyl groups are free to rotate around their $P-C_{ipso}$ axes as is evident from the observation of just one signal for both *ortho*-protons of each of the phenyl groups. The mesityl groups on the other hand show well-separated sharp signals for each of their *ortho* and *meta* substituents in the one-dimensional ^1H NMR spectra. EXSY spectroscopy shows (Figure 6, left) that the exchange process includes an exchange of the mesityl groups as a whole. During this exchange process the mesityl groups are free to rotate since EXSY correlations are observed between H29′ and H29 as well as H27. The fact that each of the *ortho*-methyl groups at one mesityl group of one isomer is found to exchange with both of the *ortho*-methyl groups of the other mesityl residue in the other isomer, implies that at some stage of the isomerisation pathway the mesityl groups are free to rotate around their $P-C_{ipso}$ axes. As the corresponding exchange peaks are of different intensity, it follows that the probability of their rotation to either side is unequal. Some exchange is also observed between the *ortho*-methyl groups of the mesityl residues which is not accompanied by their switching between pseudo-axial and pseudo-equatorial positions, i.e. within one and the same isomer (Figure 6, left; H18/H20, H27′/H29′). This exchange process is again too slow to be apparent in the corresponding one-dimensional ^1H NMR spectra.

Quantitative analysis of the EXSY data (Exp. Sect.) reveals the dynamics of the system in quite some detail. The equilibrium $\delta \rightleftarrows \lambda$ has an equilibrium constant of $K = 4.7$ at 298 K. The rate constant determined for the conversion of the δ form into the λ form is $k_{\delta\rightarrow\lambda} = 1.8\ s^{-1}$, the reverse reaction shows $k_{\lambda\rightarrow\delta} = 0.4\ s^{-1}$ (Table 7). These rate constants have been derived from a whole series of ^1H-^1H EXSY experiments, with similar values stemming from ^{31}P-^{31}P EXSY spectra (see Exp. Sect.).

The transformation of the λ isomer into the δ isomer and the transformation of the δ isomer back into the λ isomer follows two different pathways with respect to the rotational motion of the mesityl groups. On both these pathways the mesityl groups are found to rotate in opposite directions around their $P-C_{ipso}$ axes. These motions are found to be strongly coupled (Figure 7).

Figure 7 illustrates the observed position of the respective methyl groups that ensues from the two different ways of $\lambda \rightleftarrows \delta$ transformation. The rotational pathway illustrated by the right-hand side of Figure 7 is deliberately assigned the label *D*. Pathway *D* refers to the clockwise rotation of the pseudo-equatorial mesityl group II around its $P-C_{ipso}$ axis that accompanies the $\lambda \rightleftarrows \delta$ transformation. EXSY analysis can of course not differentiate between a clockwise rotation of x degrees and a counter-clockwise rotation of $360 - x$ degrees. It can, however, clearly differentiate between the individual positions of the mesityl groups in the two isomers. The absolute positions are unequivocally established by NOE data and correspond to the ones shown in Figure 7. The left-hand side of Figure 7 illustrates the second pathway on which a $\lambda \rightleftarrows \delta$ isomerisation can occur. It is labelled *L* with respect to the counter-clockwise rotation of the pseudo-equatorial mesityl group II. EXSY data also demonstrate the strongly coupled and counter-sense rotation of the two mesityl groups on this second pathway. The probability of which pathway is taken is determined as $P_L = 0.8$ and $P_D = 0.2$ (the total probability that either of the two pathways will be taken during the transformation of the λ into the δ isomer ($\lambda \rightarrow \delta$) − and the reverse transformation ($\delta \rightarrow \lambda$) − is, of course, equal to 1). These probabilities are extracted from 2D ^1H EXSY measurements of the individual rate constants and are accurate to within 10% (Exp. Sect.).

Figure 8 illustrates the overall process. Starting from a λ isomer the two isoenergetic δ isomers, δ_L and δ_D, are formed. The only difference between these two forms is a 180° rotation of the mesityl groups around their $P-C_{ipso}$ axes.

The pathways shown in Figure 8 are illustrated with respect to the transformation of a λ into a δ isomer. During the back-transformation of a δ isomer into a λ one the same pathways are, of course, taken such that the δ_L as well as the δ_D isomer will again have the choice between two different pathways when transforming back into the λ conformation. The diagram in Figure 8 illustrates the reaction sequence $\lambda \rightarrow \delta \rightarrow \lambda$. The same arguments, as illustrated for this type of process, apply to the corresponding process starting from δ passing by λ and landing again at δ. In other words, if in the diagram every λ is replaced by a δ and every δ is replaced by a λ the corresponding probabilities remain unchanged. EXSY cross-peaks that refer to the pathways illustrated in Figure 8 are observed for $\lambda_{LD}/\lambda_{DL}$ as well as for the couple δ_{LD}/δ_{DL}. The two-step transformations from λ into λ_{LL} and λ_{DD} correspond to peaks on the diagonal and

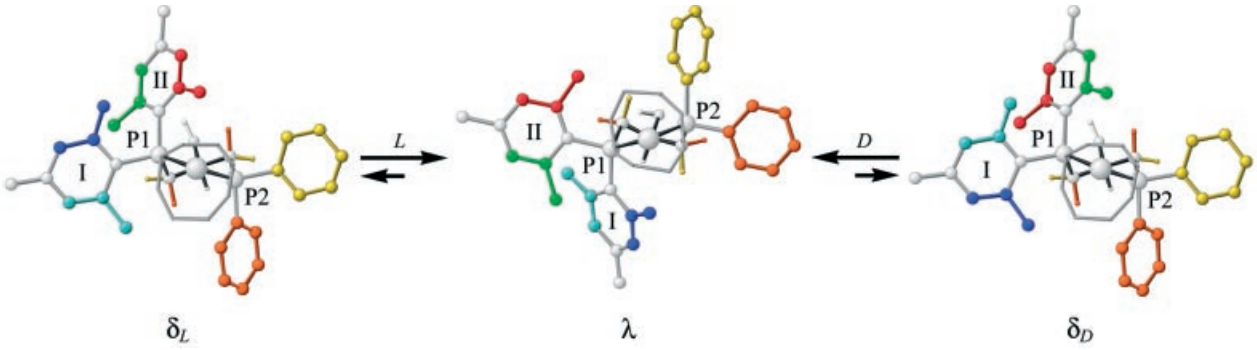

Figure 7. Coupling between λ ⇄ δ isomerisation and mesityl rotation; the rotation of the mesityl groups at a $PMes_2$ entity is strongly coupled; labels *L* and *D* for the pathways of the λ ⇄ δ isomerisation refer to the sense of this rotational process

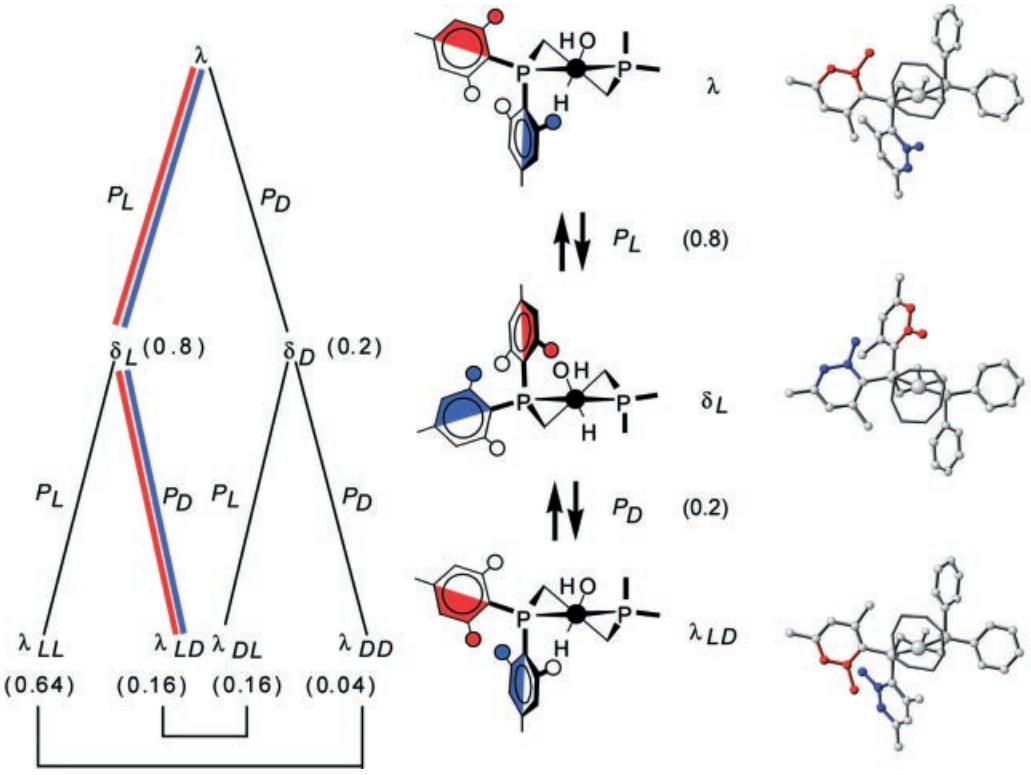

Figure 8. Probability of individual rotational motions of the mesityl groups during λ → δ/δ → λ isomerisation for **1**

are not seen directly. The fact that the couple $\lambda_{LD}/\lambda_{DL}$ can only ensue from λ by a sequence of two exchange steps is already clearly apparent from the time dependence of the corresponding 2D ^{1}H EXSY cross-peak intensity. If EXSY spectra are taken with different mixing times, single exchange processes are apparent by their nonzero slope at mixing time $\tau_m = 0$ s as well as by the linear dependence of the size of the corresponding integrals on mixing time over a range of short mixing times. Double exchange processes are, on the other hand, characterised by a zero slope at mixing time $\tau_m = 0$ s. The dependence of the corresponding integrals on time is close to parabolic instead of linear. The EXSY signals corresponding to the two-step processes $\lambda_{LD}/\lambda_{DL}$ and δ_{LD}/δ_{DL} show this parabolic dependence and zero slope at $\tau_m = 0$ s. The time dependence of the corresponding signals is correctly reproduced by the rate constants and reaction probabilities which were derived from the analysis of single-step processes (Table 7, Exp. Sect.).

With respect to the conformation of the $PMes_2$ group both pathways *D* and *L* involve a one-ring flip process.[14] This process is illustrated in Figure 9. The top half of this figure sketches the rotational reorientation undergone by the mesityl groups during a λ ⇄ δ isomerisation process following pathway *L* (major pathway). The bottom half correspondingly refers to pathway *D* (minor pathway). The diagrams show snapshots of these transformations. These snapshots have been obtained by a linear interpolation of the Rh−P−C_{ipso}−C_{ortho} torsion angles between their values in the λ and the δ isomers (X-ray structures taken as a basis). The graphs were obtained by orienting the $PMes_2$ group as a whole such that the pseudo-axial mesityl groups of the λ and δ isomers are close to vertical with the interme-

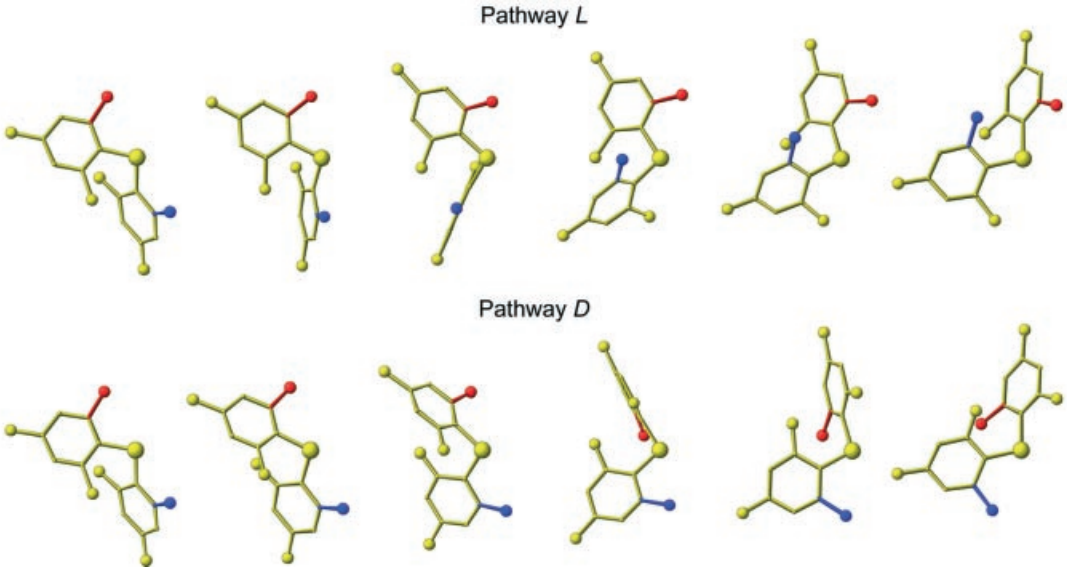

Figure 9. Illustration of the one-ring flip processes accompanying the λ ⇄ δ isomerisation for **1**; the labels *D* and *L* refer to the rotational pathways as illustrated in Figure 7

diate rotational positions again obtained by linear interpolation. The direction of view taken stays constant throughout Figure 9 and corresponds to a view along the pseudo-C_2 axis of the chelate framework. The sketches thus obtained are not to be taken as snapshots along the minimum energy pathway but they serve well to illustrate the fact that, whatever the real pathway looks like, it has to incorporate a one-ring flip process in each case.

The conformational isomerisation of **1** may thus be described as follows: δ and λ isomers interchange with one another with different rate constants (Table 7), with the λ isomer being the more stable one. The exchange process follows two different pathways with respect to the motion taken by the mesityl groups at the $PMes_2$ entity (Figure 9). There are two different types of motions both of which are such that the rotation of one mesityl group is strictly coupled to the rotation of the other mesityl group in each case (Figure 9). The barriers which correspond to these different pathways differ by approximately 4 kJ mol^{-1} at 298 K.

The same type of procedure as explicitly described for **1** was applied to compounds **2**−**4**. The corresponding data are given in the Exp. Sect. In the solid state **2** exists as just one conformational isomer [δ twist, (*R*) ligand; Figure 1].[15] For the purpose of further discussion, the argument is based on the (*S*) enantiomer of the ligand. The crystal structure of this isomer would of course correspond to the λ form (since the NMR experiments conducted are such that they do not differentiate between enantiomers in an absolute sense, this shift of reference frame has no further physical consequence; it is, however, indicated by the quest for a uniform illustration). NMR spectra show that two isomeric forms of **2** equilibrate with each other in solution. NMR structure analysis (see below, Exp. Sect.) proves that these two isomers are the λ and δ forms of the compound. At room temperature the λ isomer is the more stable one (K_{298} = 6.8). The activation barrier for the δ → λ transition amounts to $\Delta G^{\neq}_{298}$ = 68.1 kJ mol^{-1}; the barrier for the reverse transition is $\Delta G^{\neq}_{298}$ = 72.7 kJ mol^{-1} (Table 7). The process of δ ⇄ λ isomerisation is again coupled with a one-ring flip transition at the $PMes_2$ group. The process is as described for **1** and illustrated in Figure 7−9 for the case of **1**. The preference of one pathway over the other (*L* over *D*, Figure 7 and 8) is the same as observed for **1** with the relative probabilities of P_L and P_D amounting to 0.9 and 0.1.

The structure of compound **3** (Figure 1) has been determined for a crystal of the racemic compound.[9] In the solid state **3** exists as a 1:1 mixture of λ and δ forms. For the sake of a homogeneous description of the results, the arguments in this paper are based on the (*S*) enantiomer of the ligand; λ and δ isomers are clearly apparent in the NMR spectra of **3**. NMR structure analysis (see below and Exp. Sect.) shows that the λ isomer is the more stable one (K_{298} = 5.9). The barrier for the δ → λ transition is $\Delta G^{\neq}_{298}$ = 73.0 kJ mol^{-1}, and the barrier for the reverse process is $\Delta G^{\neq}_{298}$ = 77.4 kJ mol^{-1} (Table 7). As already observed for **1** and **2**, two different one-ring flip transitions are encountered along the isomerisation pathway. With respect to the illustrations given for **1** (Figure 7−9) the pathway labelled *L* is only slightly preferred over pathway *D* (P_L = 0.6, P_D = 0.4) in the case of **3**.

Compound **4** (Figure 1) exists as a 1:1 mixture of λ and δ isomers in the solid state.[8] The two isomers are also present in solution with a preference of 3:1 of the λ isomer over the δ isomer at 298 K. The activation barriers are $\Delta G^{\neq}_{298}$ = 71.6 kJ mol^{-1} for the δ → λ process and $\Delta G^{\neq}_{298}$ = 74.5 kJ mol^{-1} for the reverse transition (Table 7). With the ligand of **4** containing a $P(o\text{-anisyl})_2$ and a $P(mesityl)_2$ group different rotational orientations of the aryl groups at the PR_2 entities might in principle be apparent for both of the PR_2 groups. EXSY spectra indicate that there is also some exchange with respect to a rotation of the anisyl

groups. The corresponding EXSY peaks are an order of magnitude smaller than the ones referring to the analogous rotation of the mesityl groups. The smallness of the corresponding exchange peaks and their partial overlap with other signals excludes the quantitative analysis of this exchange. If these minor peaks are ignored and the exchange referring to the anisyl groups is correspondingly modelled as a two-site exchange process (Exp. Sect.) the resulting rate constants agree with the overall rates for the $\delta \rightleftarrows \lambda$ isomerisation process within the limits of error (Table 7). The individual probabilities for the pathways *L* and *D* are found to be $P_L = P_D = 0.5$.

Results from Dissolving Crystals of 1−7 at Low Temperatures

Crystals of **1**−**7** have been found to contain either just one conformational isomer (**2**: twist; **6**, **7**: chair) or two of them in equal amounts (**1**, **3**, **4**, **5**: λ, δ twist). If the activation barriers for the conformational isomerisation are high enough, dissolution of the crystals at low temperature should produce metastable solutions which would in the optimal case contain the conformational isomers in the same ratio as they are present in the crystals. This way an independent assignment of conformations could thus be possible. Another benefit of this type of experiment is that the rate constants of the processes as well as their dependence on temperature could be obtained in independent experiments. ^{31}P NMR spectroscopy was used as the experimental tool throughout.

As crystals of **1** contain a 1:1 mixture of λ and δ isomers, dissolution of these crystals at low temperatures is expected to produce a solution that contains the two isomers in a 1:1 ratio. The activation barriers for the $\delta \rightarrow \lambda$ and $\lambda \rightarrow \delta$ isomerisation have already been found to be above 70 kJ mol^{-1} (see above) such that at the lowest feasible temperature using CD_2Cl_2 as a solvent, isomerisation should be very slow. It is in fact observed that between 175 and 200 K the ratio with which the λ and δ isomers are contained in the solution is 1:1 [Figure 10; $\ln(c_\lambda/c_\delta) = 0$]. Above this temperature an increase of the concentration of one isomer over the other is observed. This increase upon warming the solution is observed in the temperature range between 200 and 230 K (Figure 10). From then on by rising the temperature further the isomer ratio follows an opposite trend. This behaviour is shown in Figure 10 in an $\ln(c_\lambda/c_\delta)$ vs. T^{-1} diagram.

The linear slope of the curve above 230 K indicates that an equilibrium between the two species is established at every measuring point. At the same time it is clear that the appearance of the sigmoidal curve as the temperature increases between 200 and 230 K relates to the fact that an equilibrium cannot be reached in this temperature interval within the time allotted to the experiment (ca. 3 h). The same conclusion is reached by cooling the solution from about 300 to 170 K. In the range of 300 to 230 K the slope of the $\ln(c_\lambda/c_\delta)$ vs. T^{-1} curve is linear, as was already found

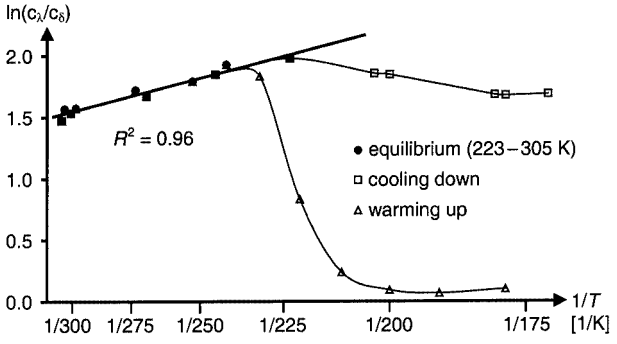

Figure 10. Isomeric ratio of **1**; the sigmoidal curve in the plot refers to ratios observed after dissolving crystals of **1** at low temperature and gradually warming these solutions (triangles); the points along the bold-face line correspond to experiments where thermal equilibrium has been reached; the open squares correspond to situations for which during cooling down equilibrium conditions could not be met; the abscissa is scaled as 1/*T*, the ordinate has a logarithmic scale

in the experiment where the temperature was increased from 230 to 300 K (Figure 10). From about 220 K on the measured ratios no longer follow the straight line but tend to level out at a value of $\ln(c_\lambda/c_\delta)$ of around 1.7 (c_λ/c_δ = 5.4). This behaviour must be due to the fact that at temperatures below 220 K equilibrium can no longer be achieved within the time given. From the slope of the straight line part of the diagram the ΔH and ΔS values relating to ΔG may be extracted; ΔS is found to be close to zero (ΔS = 1.7 J K^{-1} mol^{-1}) and ΔH amounts to −3.4 kJ mol^{-1} (Table 1).

Some information about the kinetics of the process is obtained by monitoring the time dependence of the concentration ratio c_λ/c_δ at low temperatures during the warming up experiment. From the equilibrium constant it is known that the rate constant of the forward process $\delta \rightarrow \lambda$ is about ten times larger than the rate constant referring to the back reaction. At low temperatures the mixture is far from equilibrium and the concentrations of both isomers are about equal. Evaluation of the time dependence of the c_λ/c_δ ratio at intervening temperatures leads to rate constants at these temperatures (see Exp. Sect.) such that the activation parameters for $\delta \rightleftarrows \lambda$ interconversion may be estimated (Table 1); $\delta \rightarrow \lambda$ isomerisation corresponds to $\Delta H^{\neq}$ = 60.5 kJ mol^{-1}, $\Delta S^{\neq} = -37$ J K^{-1} mol^{-1}, with the reverse reaction being characterised by $\Delta H^{\neq}$ = 64.4 kJ mol^{-1}, $\Delta S^{\neq} = -36$ J K^{-1} mol^{-1} (Table 1).

Similar experiments have been performed for compounds **2**−**7** (see Supporting Information) leading to estimates of thermodynamic and kinetic parameters as given in Table 1.

Quantitative NMR Spectroscopic Structure Analysis

While all NMR spectroscopic data show that compounds **1**−**7** exist as mixtures of two conformational isomers in solution, it is not clear from the beginning which conformation corresponds to which isomer. In the case of **2** the experiments referring to the dissolution of a crystalline

sample of **2** at low temperatures (see preceding paragraph) could decide between the λ and δ forms of this compound and an absolute assignment was thus possible.

As a general tool to assign definite conformations to the different isomers, distance geometry (DG) methods were applied to compounds **1**−**4**. Based on the ^{1}H NOE data (Table 8, Figure 5) restraints on interproton distances were defined in each case. The initial structural models were chosen as the λ and δ conformations, the structure of which is basically known from X-ray data. It was found that the results obtained were quite independent of whether those starting conformations were taken as the X-ray determined conformations themselves or as the appropriate conformations as modelled by the ESFF force field.[16] It was also found that when starting from a modelled chair conformation, which is quite improbable on the basis of the X-ray results, the final distance geometry determined conformations were the same as the ones reached from the other starting points. For the final calculations the X-ray determined models were used as the starting point. These calculations were performed for the major and for the minor isomer in each case. For each of the two conformational isomers observed in solution for compounds **1**−**4** both λ and δ twist conformations were chosen as the starting points.

For distance geometry refinement different strategies can be applied dependent on the amount of variation allowed to the NOE-derived restraints. With weak restraints, corresponding to a large amount of variation being permitted, λ and δ forms can interchange into one another. In order to discriminate between the two principle possibilities the resulting optimised conformations have to be sorted into λ and δ classes after refinement. The calculated NOE distances for these refined structures may then be compared with the experimental ones in order to decide whether λ or δ gives the better fit. Another strategy that was applied throughout for the calculations reported here consists of using strong NOE restraints, i.e. variations allowed only to within ±5% with respect to the NOE determined distances. With this strategy λ and δ forms cannot change into one another such that two sets of optimised structures are finally obtained, one exclusively containing conformations with a λ twist and the other one with only δ conformations. In the case of the major isomer it was observed for all compounds **1**−**4** that the rms values as calculated by the error function of the DG programme[17,18c,29a] were about one order of magnitude different for the two classes. The class relating to the lower rms values should then be the one to which the isomer belongs. Different types of qualifiers may be used to ascertain this decision (Exp. Sect.). All of them unequivocally lead to the same result, i.e. the λ isomer is the more stable one throughout (Exp. Sect., Table 8, 9). This result shows the power of distance geometry methods in assigning conformations. There is only one proton (H3;

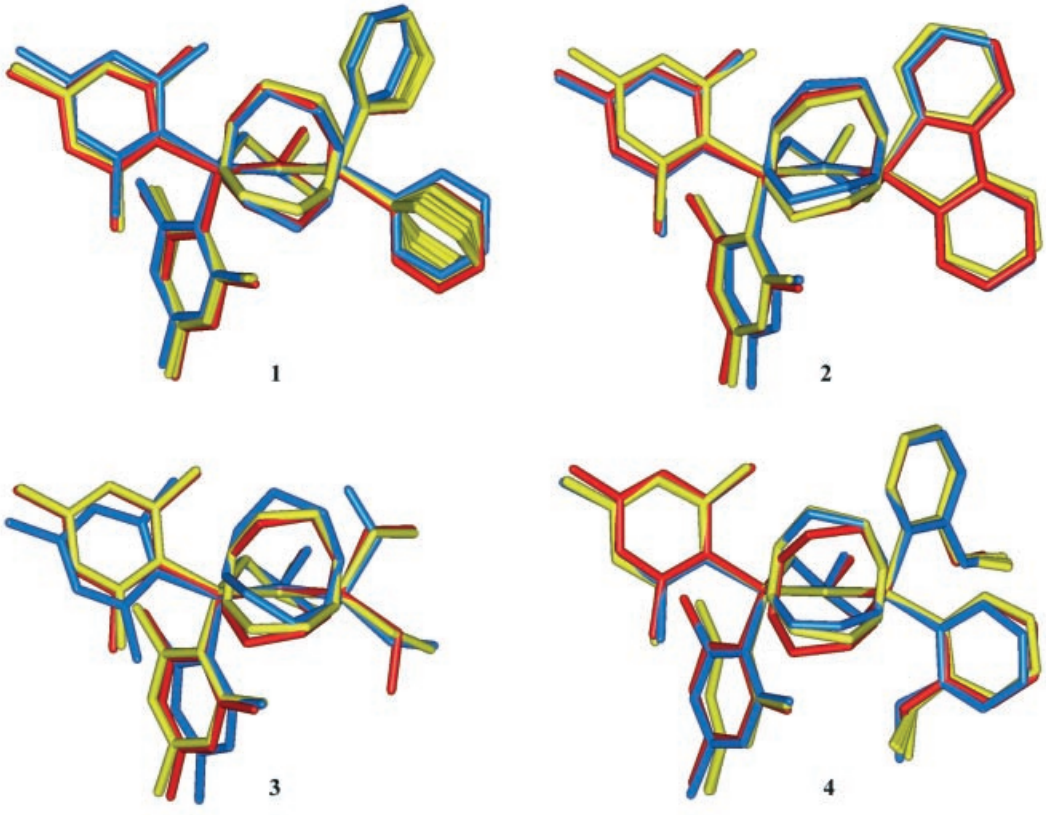

Figure 11. Overlay of the conformations of **1**−**4** (λ twist form) as inferred by different techniques; colour code: blue: X-ray structure; red: optimal single conformation as derived from force field refinement; yellow: DG-derived conformations

Figure 2 and 3 and 5), the proton at the chiral carbon atom, that directly pinpoints to λ and δ conformations. A sufficient number of NOE contacts involving H3 could be determined for each of the compounds **1**−**4** for the major isomer, and these contacts are most important in differentiating between λ and δ forms. For the minor isomer only a smaller number of contacts was experimentally accessible in each case. Nevertheless, applying the same procedure as described for the major isomer did not lead to any contradiction of the conclusive results obtained for the major isomer in each case. Whenever the major isomer was found to have a λ conformation, as was the case for each of the compounds **1**−**4**, the set of solutions obtained for the minor isomer by distance geometry refinement had a better fit for the models with δ conformation than for the ones with λ conformation (Exp. Sect., Table 9). This means that even with the small number of NOE contacts found for the minor isomer in each case, distance geometry methods are able to differentiate between λ and δ forms of the chelate cycle.

It is found throughout (Figure 11) that the average structure in solution conforms nicely to the structure in the solid state. This is shown in Figure 11 for all compounds **1**−**4** for the major isomer. The scatter of conformations as inferred from the results of DG runs is also shown in Figure 11.

It is seen that the only parts that are rotationally flexible to a higher or lesser degree, are the phenyl residues (**1**), the ethyl groups (**3**), and the methoxy groups (**4**). It is also seen that the conformations of **2** containing the DBP residue show no scatter at all. The graphs in Figure 11 also show a comparison with the structure of the least-energy model obtained in each case by force field refinement. Again, the difference between the solid state conformations and the force field calculated conformations is quite small in all cases; all three models, X-ray, DG refinement, and force field refinement are almost exactly congruent for **2** which means that due to steric repulsions and the fixed geometry of the DBP group this conformation finds itself in a minimum of the corresponding energy hypersurface which has steep ascents in all directions.

Discussion

An important result of this study is that it is found that structures determined by X-ray methods in the solid state and structures characterising the ensembles of molecules in solution are congruent within the limits of error. This gives much credit to the application of NMR spectroscopic structure analysis − which has been so successful in protein structure assignment[18] − also with small molecules. Even if the number of discriminative NOE contacts is much smaller in small molecules than it is in proteins (due to the fact that amino acids, which are far apart in a sequence,

Table 1. Thermodynamic and activation parameters for **1**−**7**

[a]		ΔH[b] [kJ mol^{-1}]	ΔS[b] [J K^{-1} mol^{-1}]	ΔG_{298} [b] [kJ mol^{-1}]	K_{298} [b]	$\Delta H^{\neq}$ [kJ mol^{-1}]	$\Delta S^{\neq}$ [J K^{-1} mol^{-1}]	$\Delta G^{\neq}_{298}$ [kJ mol^{-1}]
1	δ → λ λ → δ	−3.4(2)	1.7(9)	−3.9	4.7	60.5(20)[c] 64.4(18)[c]	−36.5(70)[c] −35.9(70)[c]	71.4[c] 75.1[c]
2	δ → λ λ → δ	−7.5(3)	−10.1(13)	−4.5	6.3	−	−	68.6 73.3
3	δ → λ λ → δ	−1.8(1)	8.4(5)	−4.3	5.7	65.8(12)[c] 67.4(11)[c]	−25.9(50) [c] −35.5(40) [c]	73.6[c] 78.0[c]
4	δ → λ λ → δ	−1.6(1)	4.2(4)	−2.8	3.1	−	−	72.1 75.0
5	A → B[d] B → A[d]	−0.5(1)	−0.6(4)	−0.3	1.2	53.2(15)[e] 53.7(15)[e]	5.0(60)[e] 5.6(60)[e]	51.7[e] 52.1[e]
6	A → B[d] B → A[d]	0.0(3)	3.8(13)	−1.2	1.6	41.4(10)[e] 41.4(10)[e]	−47.0(40)[e] −50.7(40)[e]	55.4[e] 56.5[e]
7	A → B[d] B → A[d]	−5.0(2)	−9.1(9)	−2.3	2.7	50.2(19)[e] 55.1(19)[e]	−31.1(70)[e] −22.1(70)[e]	59.4[e] 61.7[e]

[a] The estimated standard deviation in units of the least significant digit is given in parentheses. [b] The signs of the thermodynamic parameters refer to the process minor isomer ⇄ major isomer. [c] Values refer to Eyring plots which were based on the rate constants measured at higher temperatures by EXSY methods (Table 7) and rate constants determined under nonequilibrium conditions (**1**: T [K], $k_{\delta\rightarrow\lambda}$ [s^{-1}], $k_{\lambda\rightarrow\delta}$ [s^{-1}]: 221, 2.4·10^{-4}, 0.3·10^{-4}; 232, 1.8·10^{-3}, 0.3·10^{-3}; **3**: T [K], $k_{\delta\rightarrow\lambda}$ [s^{-1}], $k_{\lambda\rightarrow\delta}$ [s^{-1}]: 212, 1.3·10^{-5}, 0.2·10^{-5}; 224, 7.1·10^{-5}, 1.0·10^{-5}; 235, 5.2·10^{-4}, 0.8·10^{-4}). The $\Delta G^{\neq}_{298}$ values thus calculated are in close agreement to the ones determined from EXSY measurements alone. [d] A: minor isomer, B: major isomer; the exact geometry in solution has not been determined. For the solid state structures see Figure 1. [e] Activation parameters refer to Eyring plots based on rate constants determined by line shape analysis of ^{31}P NMR spectra.

may be in close contact to each other due to the folding of the proteins while constituents of a small molecule which are separated by a far smaller number of intervening atom−atom distances are rarely found to be in close contact to each other) this small number of contacts is still sufficient to determine the structure of small molecules as well.

The refinement of structural models as developed by DG methods has to make use of force field calculations. It appears that the general ESFF force field[16] is well parameterised for this purpose as seen by refining the X-ray derived models by these methods. Almost negligible changes of the conformations are observed in this case. It is also satisfying to note that the energy differences between the λ and δ isomers as calculated by the force field approach in each case are in the same order of magnitude as the ones which have been experimentally determined (Table 1). The calculated energy differences are $\Delta E = E_\lambda - E_\delta = 2.1$, -0.2, 6.1, and -2.5 kJ mol^{-1} in the series of compounds **1**−**4**. Comparison with the experimental ΔH values in Table 1, shows that the calculated values do not correctly predict which of the two forms is the more stable one nor do they rank the compounds correctly with respect to these energy differences. Since force field methods have been found to be quite appropriate for the calculation of such small energy differences in the stereochemistry of organic ring compounds[19] it is evident that it is not the force field method in itself which leads to wrong results in the case of **1**−**4** but that the parameterisation of these methods is not yet good enough for metal-containing compounds.

As far as the energy differences between the two conformers are concerned they are found to be in a small range for all compounds **1**−**7**. It is seen that the larger the steric discrimination between the two different PR_2 groups is [$PMes_2/PEt_2$ (**3**), $PMes_2/PPh_2$ (**1**), $PMes_2/P(o\text{-anisyl})_2$ (**4**)] the more the equilibrium will lie on the side of the λ twist form (Table 1). The λ twist form is even more preferred by **2** with its $PMes_2$ substituent on one side and a dibenzophospholyl group on the other side. The rigidity of the DBP residue obviously causes less interference within the molecule than even a PEt_2 group (Table 1). The almost 1:1 equilibrium between the two forms of **5** [$P(o\text{-anisyl})_2/PMes_2$] indicates that the steric influence of these two groups onto the chelate cycle is not greatly different. For compounds **6** and **7** [$P(o\text{-Tol})_2/PPh_2$ (**6**), $P(o\text{-Tol})_2/PEt_2$ (**7**)] the lesser steric demand of PEt_2 in comparison to PPh_2 again mirrors itself in the equilibrium constants with the equilibrium referring to **7** being more biased ($K = 2.7$) than the one referring to **6** ($K = 1.6$). Due to the differences in the entropic terms the ΔG_{298} values show a smaller difference amongst the series of compounds than do the ΔH values such that the equilibrium constants K_{298} are in the narrow range of 1.2−6.3.

Throughout the series of compounds **1**−**4** the λ isomer is the more stable one. The reason for this is intuitively clear from looking at the structural models (Figure 11) where it is seen that the C−O bond at the central carbon atom of the ligand is tilted such as to orient it away from the mesityl side of the compounds, i.e. away from the bulkier of the two PR_2 groups (Figure 11).

The activation barriers are higher than those normally found in saturated organic ring compounds (ca. 30 kJ mol^{-1} higher than in cyclohexane).[20] The activation entropies are definitely negative for the two compounds for which they could be determined (**1**, **3**). This indicates that sterically highly crowded situations are met along the transition pathway.

For all compounds **1**−**7** data about the efficiency in catalysing the enantioselective hydrogenation of (*Z*)-2-acetamidocinnamic acid are available.[8] No direct correlation between the reported *ee* values[8] and any of the thermodynamic and kinetic data reported in this paper is apparent. Thus, it has been found that compound **5** is the most enantiodiscriminating catalyst leading to *ee* values of the hydrogenation product of up to 85% *ee*[8] while the two isomers of this compound are present in a close to 1:1 ratio at the temperature of catalysis (298 K). Compounds **1** and **2** which show a strong predominance of the λ conformation (Table 1) produce *ee* values of only 40−60%.[8] Compound **6**, for which both conformations have equal enthalpies (Table 1) and for which the major/minor equilibrium is close to 1:1, yields the hydrogenation product with around 50% *ee*.[8] It is thus clear that the thermodynamic equilibrium of the λ and δ forms of the precatalyst has no direct bearing on the chirality of the transition state of the hydrogenation reaction. Table 1 and the data published on the catalytic activity of **1**−**7**[8] allow for the following hypothesis. Since both compounds **6** and **7** have a chair conformation in the solid state and are at the same time least efficient in enantiodiscrimination it appears probable that twist conformations are a prerequisite for an efficient enantioselective catalyst. Compounds **1**−**5** show twist conformations in their solid state structures. For compounds **1**−**4** the persistence of twist conformations in solution is proved in this paper. For compound **5** this persistence is not proven by NMR spectroscopic analysis but highly probable. Compound **5** is the most efficient enantioselective catalyst amongst compounds **1**−**5**. On the other hand **5** is a compound where the two forms (presumably λ and δ twist) are of almost equal stability (Table 1). A high degree of enantioselectivity as found for **5** can therefore not ensue from the predominance of one of the two chiral forms of **5** over the other. Enantiodiscrimination must then be due to an induced fit between the prochiral substrate and the chiral coordination scaffolding.[21] For this type of fit, as induced by the substrate, consisting of switching from λ to δ twist conformations or vice versa, it is seen from Table 1 that amongst the enantiodiscriminating catalysts **1**−**5** compound **5** is the one with the lowest activation barrier for this switching process. It may then be argued that a prerequisite for an efficient enantiodiscriminating catalyst is the intrinsic stability of its λ and δ twist forms as well as a low barrier for the transformation between these forms such that a prochiral substrate may easily induce the appropriate fit.

Conclusion

Compounds $[\{\kappa\text{-}PR_2CH_2CH(OH)CH_2\text{-}\kappa\text{-}PR'_2\}Rh(\eta^4\text{-}COD)]^+PF_6^-$ exist as λ and δ conformers when at least one of their PR_2 groups is a $PMes_2$ entity. As shown by quantitative NMR spectroscopic structure analysis their conformations in solution correspond to the conformations adopted by them in the solid state. From the two conformations the one which is preferred is that which keeps the central C−O bond of the chelate ligand away from the mesityl side. The experimentally determined difference between the enthalpy of the two isomers is found to lie within a few kJ mol^{-1} with ΔS values in the range of ± 10 J K^{-1} mol^{-1}. The free energies of activation for the conformational changes (δ → λ and λ → δ) are around 70 kJ mol^{-1}. Negative activation entropies indicate the steric strain along the reaction pathway. The mesityl groups at the $PMes_2$ entity behave as coupled rotors, their rotation is only possible in the transformation between λ and δ forms. Due to the chirality of the compounds the probabilities with which rotation in either sense will occur are not generally equal. The rotational pathways taken correspond to one-ring flip processes in each case. The precise thermodynamic data worked out in this paper may serve as criteria to evaluate force field models that describe the compounds in the sense of a mechanical molecular machine.[22]

Experimental Section

General Remarks: Bruker instruments of the type DPX200 operating at 200.13 (^{1}H), 81.014 MHz (^{31}P), DRX300 at 300.13 MHz (^{1}H), 75.468 (^{13}C), 121.495 MHz (^{31}P), and DRX500 at 500.13 (^{1}H), 125.758 (^{13}C), 202.456 MHz (^{31}P) were used throughout. Chemical shifts are given in ppm with respect to CD_2Cl_2 (^{1}H: δ = 5.32 ppm; ^{13}C: δ = 53.5 ppm) as internal standard. ^{31}P chemical shifts are expressed in ppm with respect to an aqueous solution of H_3PO_4 (85%) as external standard. All measurements were performed on samples dissolved in CD_2Cl_2 under argon in sealed NMR tubes. The dissolution of crystalline material at low temperature was performed as follows: NMR tubes were fixed to a vacuum line. The crystalline sample was introduced into the tube under argon and the tube was immersed into a liquid N_2 bath. CD_2Cl_2 was condensed onto it and the tube was sealed. The solid material (sample and CD_2Cl_2) was allowed to warm up to 160 K and transferred at this temperature into the NMR probehead. The temperature of the probehead was gradually increased until the shape of the ^{31}P NMR resonances showed that the sample had completely dissolved. The temperature was calibrated using [D_4]methanol (99.8%) and ethylene glycol samples.[23]

Measurement Techniques and Assignment: Standard pulse sequences were applied throughout. The acronyms given in Table 2 refer to the standard Bruker pulse sequence library. By a combination of 1D and 2D NMR spectroscopic experiments (Table 2) unequivocal assignment of the NMR resonances of the two isomers was possible for **1**−**4**. NMR spectroscopic data referring to **1** are shown in Table 3 and 4. NMR spectroscopic data for **2**−**4** are available as Supporting Information. For compounds **5**−**7** analysis was based on ^{31}P NMR spectra alone. The complete set of ^{31}P NMR spectroscopic assignments for **1**−**7** is given in Table 5. The peak volumes of 2D NMR spectra were measured by the volume integration algorithm supplied with the FELIX NMR spectroscopic processing software package.[24] 2D ^{1}H NOESY/EXSY data were collected with different mixing times (see Table 2) at 298 K throughout. For the purpose of quantitative interpretation of the ^{1}H NOE data the initial rate approximation was chosen.[25] The dependence of the peak volumes on mixing time was first analysed by the inspection of the corresponding graphs (Figure 12, right). Based on this inspection it was decided how many measuring points should be included for obtaining the slope in a linear fit. The peaks above and below the diagonal were analysed separately. Further evaluation was based on the one of the two graphs that showed the larger slope. In general the volume of the corresponding peaks above and below the diagonal were in good agreement (Figure 12, right).^{1}H EXSY peaks were evaluated by the same type of procedure (Figure 12, center), where the average of the volume integrals of the peaks above and below the diagonal, was used. To evaluate the rate constants the slope based on the values obtained for a mixing time of $\tau_m = 50$ ms was used throughout, since it was found that internal consistency of the rate data decreases if longer mixing times within the "linear" first part of the curve (Figure 12, center) are incorporated in calculating the slope. The volume integrals of the diagonal peaks showed the expected continuous decrease with increasing mixing time as seen from the curves in Figure 12 (left). A single exponential fit (solid line) is not completely appropriate especially at short mixing times. It was decided therefore to use the two integrals corresponding to the shortest and the next shortest mixing times (Figure 12, left) in a linear extrapolation in order to estimate the integral value at mixing time $\tau_m = 0$ s. 2D ^{31}P EXSY data were collected with mixing times of 100−600 ms at 298, 300, and 305 K. Volume integrals collected with mixing times of up to 400 ms were found to be far enough away from saturation such as to allow kinetic data to be extracted from them.

Coupling Constants: Since the experiments on **1**−**4** make it clear that the major isomer corresponds to the λ twist conformation of the chelate ring in each case and since the structure of the twist conformations is known from X-ray analysis as well as from modelling and NOE data, the torsion angles H−C−C−H, H−C−C−P

Table 2. Experimental details of the 2D NMR experiments for **1**−**4**

	DQF-COSY	^{1}H-^{31}P HMBC	^{1}H-^{13}C HSQC	^{1}H-^{13}C HMBC	^{1}H NOESY/EXSY	^{31}P EXSY
Pulse program[a]	cosygsmftp	inv4gslrnd	invietgssi	inv4gslplrnd	noesytp	noesydctp
TD (*F*2/*F*1)	4096/256	2048/128	2048/256	2048/256	4096/256	2048/128
NS	32	24	16	32	16	32
τ_m [ms]	−	25−180	−	60−80	50−800	100−600
D1 [s]	1.7	1.6	1.6	1.5	2.0	2.0

[a] The acronyms in this row refer to pulse programmes supplied under these names for the BRUKER Avance DPX/DRX series of instruments.

Table 3. ^{1}H NMR spectroscopic data of **1**

λ isomer[a] Major	δ(^{1}H)	Pattern ^{1}H	$^nJ_{H,H}$/($^nJ_{HP}$) [Hz]	δ isomer[a] Minor	δ(^{1}H)	Pattern ^{1}H	$^nJ_{H,H}$/($^nJ_{HP}$) [Hz]
H37,41$_{ax}$	8.16	ddd	7.1/(11.4/1.0)	H31′,35′$_{ax}$	8.08	dd	7.2/(10.3)
H39$_{ax}$	7.70	m	7.3/1.0	H33′$_{ax}$	7.69	ov	
H38,40$_{ax}$	7.64	m	8.0/1.1	H32′,34′$_{ax}$	7.66	ov	
H33$_{eq}$	7.49	m	7.1/(1.5)	H39′$_{eq}$	7.48	m	
H32,34$_{eq}$	7.44	m	7.6/(2.0)	H38′,40′$_{eq}$	7.46	ov	
H14$_{ax}$	7.26	br. d	(3.7)	H25′$_{ax}$	7.29	d	(3.7)
H31,35$_{eq}$	7.11	ddd	6.8/1.1/(9.5)	H37′,41′$_{eq}$	7.16	dd	7.3/(9.8)
H25$_{eq}$	7.04	br. s		H16′$_{eq}$	7.04	ov	
H16$_{ax}$	6.94	br. s		H23′$_{ax}$	6.96	s	
H23$_{eq}$	6.79	br. s		H14′$_{eq}$	6.79	ov	
H4	4.77	br. m	11.5/7.3	H5′	4.79	ov	12.5
H8	4.46	br. m	11.6/7.4/(4.1)	H9′	4.48	ov	15.0
H9	4.33	br. m	12.2/6.6	H8′	4.28	ov	15.0
H5	3.92	br. m	12.4/7.4/(4.1)	H4′	4.01	m	12.0/6.8
H3	3.63	m	10.6/6.0/(12.0)	H3′	3.82	m	8.2
H18$_{ax}$	3.52	s		H29′$_{ax}$	3.56	s	
H11$_{eq}$	3.07	dddd	13.7/5.6/2.3/(10.2)	H12′$_{eq}$	2.93	m	15.4/6.2
H29$_{eq}$	2.68	s		H20′$_{eq}$	2.64	s	
H12$_{ax}$	2.62	m	14.1/10.1	H11′$_{ax}$	2.73	dd	15.4/6.7
H111	2.58	m	14.2/6.8	H61′	2.55	ov	
H101	2.50	m		H71′	2.48	ov	
H22$_{eq}$	2.49	m	15.4/1.7	H21′$_{eq}$	2.67	ov	13.8/9.1
H19$_{ax}$	2.37	s		H28′$_{ax}$	2.38	ov	
H112	2.36	m	9.7/6.8	H62′	2.36	ov	
H71,72	2.33	m		H101′,102′	2.37	ov	
H28$_{eq}$	2.27	s		H19′$_{eq}$	2.27	ov	
H102	2.23	m	12.8/6.3	H72′	2.22	ov	
H21$_{ax}$	2.17	ddd	15.4/7.1/(1.8)	H22′$_{ax}$	2.05	ov	13.8/11.3
H61,62	2.13	m	16.4/10.6	H111′,112′	2.19	ov	
H20$_{ax}$	2.01	s		H27′$_{ax}$	2.05	s	
HO	1.74	d	4.7	HO′	1.43	d	8.8
H27$_{eq}$	1.66	s		H18′$_{eq}$	1.65	ov	

[a] Labels refer to Figures 3 and 4; measuring frequency: 500.13 MHz; temperature: 298 K; solvent: CD_2Cl_2; observed signal pattern abbreviations: s = singlet, d = doublet, t = triplet, m = multiplet, ov = overlapping signal, br. = broad.

and H−C−P−C can be calculated for both the λ twist and δ twist forms of each of the compounds **1**−**4**. The torsion angles allow the degree of ^3J coupling to be predicted in each case. Determination of the corresponding coupling constants is in part possible by 2D NMR spectroscopic experiments. Even in the case where a numerical value of an individual coupling constant cannot be obtained with sufficient accuracy, the relative degree of coupling may be inferred from the size of the corresponding volume integrals. If the observed degree of coupling is ranked as strong (*s*), medium (*m*) and weak (*w*) a comparison of the ranking derived from calculated torsion angles and the ranking derived from NMR spectroscopic experiments is possible. This type of comparison is shown in Table 6 for the λ twist isomer of **1** as an example. It is seen that on the basis of $^3J_{H,H}$ coupling the agreement between calculated and experimental degrees of coupling is definitely better for the values calculated for the λ twist isomer than for the ones derived from the geometry of the δ twist isomer. It is also seen that the $^3J_{HP}$ and $^3J_{HC}$ couplings do not differentiate between the two twist isomers. If on the other hand a chair conformation of the chelate cycle is chosen as the basis of comparison (Table 6) almost all of the experimental $^3J_{HX}$ couplings show a definite misfit. It is seen then that the $^3J_{HX}$ couplings strongly indicate that the solution structure of the major isomer of **1** adopts a twist conformation while only the $^3J_{H,H}$ couplings involving H3 (Figure 3) allow to differentiate between its λ twist and δ twist forms. The λ twist form that in fact corresponds to the conformation of the major isomer gives the best agreement, as expected. The same type of analysis, when performed for the minor isomer of **1,** shows a better fit for the δ twist isomer ($^3J_{H,H}$ coupling constants 6.2, 6.7, 11.3, 9.1 Hz in the sequence shown in Table 6, ranking of couplings: *m*, *m*, *s*, *m*). For compounds **2**−**4** the observed degree of $^3J_{HX}$ coupling is also in agreement with the conformations assigned to the individual isomers in each case (see Supporting Information).

Evaluation of Kinetic Data and Thermodynamic Parameters: The rate constants for the overall process of δ ⇄ λ isomerisation were evaluated by the method of exchange between two unequally populated sites.[26] In the case of the ^{31}P EXSY data this evaluation was based on the molar fraction approach.[26] For the ^{1}H EXSY data this approach as well as the evaluation using the integral values at zero mixing time were used, with only slight differences in the resulting rate constants which were found to be within the margins of error.

The protons of the mesityl groups are involved in a four-site exchange throughout. The mesityl groups are allowed to rotate only in connection with a δ ⇄ λ exchange; thus, in one exchange step a specified mesityl proton may exchange with two mesityl protons of the product; a consequent reverse reaction will then lead to an exchange with a proton of the mesityl group in the starting conformation. The rate data corresponding to these processes were evaluated by finding the solution to the four corresponding linear differential equations according to standard methods.[27] For the corresponding matrix operations MATHEMATICA[28] was used as the tool.

Table 4. $^{13}C\{^1H\}$ NMR spectroscopic data of **1**

λ isomer[a] Major	δ(^{13}C)	Pattern $^{13}C\{^1H\}$	$^nJ_{C,P}/(^nJ_{CRh})/[^1J_{CH}]$ [Hz]	δ isomer[a] Minor	δ(^{13}C)	Pattern $^{13}C\{^1H\}$	$^nJ_{C,P}/(^nJ_{CRh})$ [Hz]
$C17_{ax}$	144.33	d	(1.3)	$C22'_{ax}$	144.94	m	
$C15_{ax}$	142.83	d	2.0	$C24'_{ax}$	142.93	d	1.7
$C13_{ax}$	141.57	d	19.5	$C26'_{ax}$	141.35	ov	
$C22_{eq}$	141.49	d	7.0	$C13'_{eq}$	141.29	ov	
$C24_{eq}$	141.13	d	2.1	$C15'_{eq}$	141.00	ov	
$C26_{eq}$	140.12	d	9.5	$C17'_{eq}$	139.66	d	9.3
$C37,41_{ax}$	136.10	d	13.3	$C31',35'_{ax}$	135.35	d	11.9
$C39_{ax}$	133.06	d	2.1	$C33'_{ax}$	133.20	d	2.5
C30/C36	132.60	m	17.4/8.9	C30′/C36′	132.52	ov	
$C25_{eq}$	132.47	d	8.3	$C16'_{eq}$	132.28	ov	
C30/C36	132.27	d	18.2/9.7/(2.6)			ov	
$C23_{eq}$	132.14	d	7.5	$C14'_{eq}$	132.26	ov	
$C16_{ax}$	131.86	d	6.6	$C23'_{ax}$	131.96	ov	
$C14_{ax}$	131.81	d	8.7				
$C33_{eq}$	131.10	d	2.1	$C39'_{eq}$	131.29	d	1.7
$C31,35_{eq}$	130.40	d	8.3	$C37',41'_{eq}$	130.17	d	10.2
$C38,40_{ax}$	129.89	d	10.8	$C32',34'_{ax}$	129.86	m	
$C32,34_{eq}$	129.61	d	9.1	$C38',40'_{eq}$	129.68	m	
$C12_{ax}$	125.30	d	41.9	$C21'_{ax}$	125.42	d	36.5
$C21_{eq}$	124.65	d	37.7				
C9	106.83	dd	9.0	C8′	107.76	dd	7.2/(9.0)
C5	99.57	dd	7.3/(7.4)	C4′	99.12	ps. t	8.5/(7.0)
C4	94.89	ps. t	8.3/(7.4)	C5′	94.04	ps. t	8.1/(8.7)
C8	92.35	dd	11.2/(6.9)	C9′	93.04	dd	11.4/(6.7)
C3	65.68	d	3.7/1.7	C3′	65.87	m	6.4
C1	34.63	dd	27.2/20.9	C1′	33.13	dd	27.1/10.2
C10/C11	31.51	d	1.2	C6′/C7′	31.57	s	
C10/C11	31.17	s	1.7	C6′/C7′	31.21	ov	
C6/C7	30.72	m	2.5				
C2	30.57	m	25.3/10.0	C2′	30.64	ov	
C6/C7	30.39	m	4.2	C10′/C11′	30.47	ov	
$C18_{ax}$	27.02	dt	12.2/(2.6)/[125.0]	$C29'_{ax}$	26.77	m	10.2/(2.7)
$C29_{eq}$	25.64	d	5.9/[127.0]	$C20'_{eq}$	26.00	d	5.1
$C27_{eq}$	24.73	d	5.0/[128.0]				
$C20_{ax}$	22.44	d	3.3/[127.0]	$C20'_{ax}$	23.12	d	3.4
$C19_{ax}$	21.04	s	[127.0]	$C19'_{ax}$	21.06	s	
$C28_{eq}$	20.83	s	[127.0]	$C28'_{eq}$	20.80	s	

[a] Labels refer to Figures 3 and 4; measuring frequency: 125.758 MHz; temperature: 298 K; solvent: CD_2Cl_2; observed signal pattern abbreviations: s = singlet, d = doublet, t = triplet, m = multiplet, ov = overlapping signal, ps. = pseudo.

Table 5. $^{31}P\{^1H\}$ NMR spectroscopic data of **1**−**7**

[a]	R^1	R^2	T [K]		δ(P^1)	$^1J_{RhP1}$ [Hz]	δ(P^2)	$^1J_{RhP2}$ [Hz]	$^2J_{PP}$ [Hz]	Conformation[b]
1	Mes	Ph	299	major	−2.57	133.2	6.74	148.0	36.1	(*S*)-λ
				minor	−4.81	131.3	10.84	149.8	36.1	(*S*)-δ
2	Mes	DBP	299	major	−1.11	134.0	6.58	144.6	37.0	(*S*)-λ
				minor	−0.05	131.7	11.49	145.9	38.6	(*S*)-δ
3	Mes	Et	299	major	−3.29	136.2	2.56	141.2	35.7	(*S*)-λ
				minor	−2.39	134.8	7.23	140.5	36.0	(*S*)-δ
4	Mes	2-MeOPh	301	major	−3.79	134.1	8.26	148.0	33.8	(*R*)-λ
				minor	−6.99	132.7	12.03	150.3	33.8	(*R*)-δ
5	2-MeOPh	Ph	182	major	11.83	143.2	11.30	142.8	46.2	−
				minor	15.65	145.8	7.52	140.7	46.5	−
6	*o*-Tol	Ph	192	major	18.13	141.9	11.68	144.2	42.7	−
				minor	15.28	143.9	14.46	139.8	42.4	−
7	*o*-Tol	Et	224	major	24.73	141.1	7.25	138.2	42.3	−
				minor	20.61	141.2	11.08	136.7	41.4	−

[a] Measuring frequency: 202.456 MHz; solvent: CD_2Cl_2. [b] The configuration of the chelate ligand was chosen such as to make a homogeneous and consistent description of all the compounds **1**−**4** possible (see text).

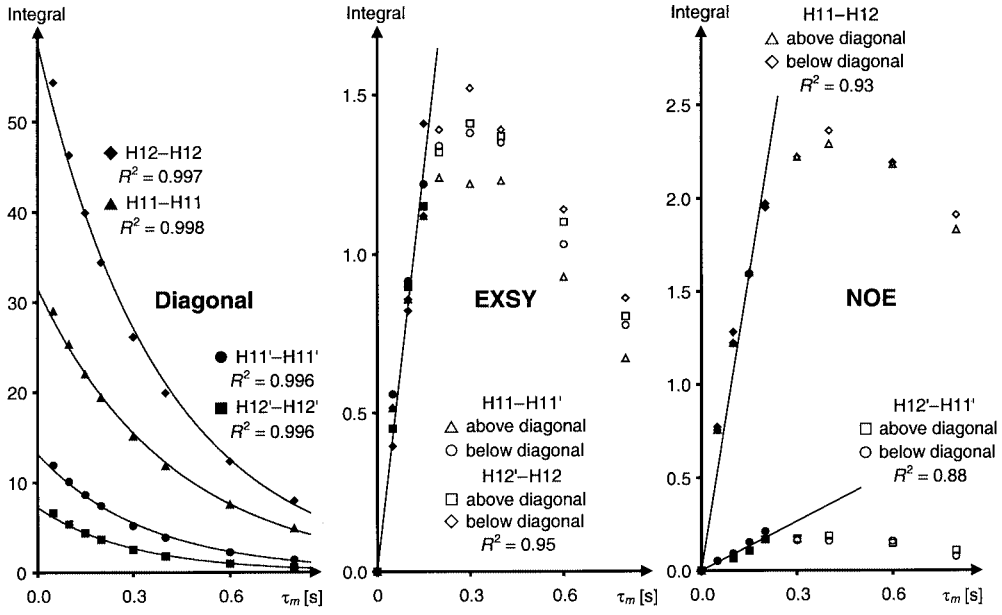

Figure 12. Characteristic time dependence of different types of peaks in 2D ^{1}H NOESY/EXSY experiments

Table 6. Comparison of the calculated and observed degrees of $^3J_{HX}$ coupling for the major isomer of **1**[a]

^{1}H DQF COSY	(*S*)-λ		(*S*)-δ				major	$^3J_{HH}$
Torsion	[°]	Torsion	[°]	λ	δ	chair	NMR	[Hz]
$H3_i-H11_{eq}$	−54	$H3'_i-H12'_{eq}$	−75	*m*	*w*	*w*	*m*	8.3
$H3_i-H12_{ax}$	−169	$H3'_i-H11'_{ax}$	39	*s*	*m*	*s*	*s*	10.9
$H3_i-H21_{ax}$	−24	$H3'_i-H22'_{ax}$	155	*m*	*m*	*s*	*m*	7.0
$H3_i-H22_{eq}$	91	$H3'_i-H21'_{eq}$	38	*w*	*m*	*w*	*w*	–
^{1}H,^{31}P-HMBC								
$H3_i-P1$	69	$H3'_i-P1'$	159	*m*	*m*	*m*	*w*	
$H3_i-P2$	−144	$H3'_i-P2'$	−86	*m*	*w*	*m*	*m*	
^{1}H,^{13}C-HMBC								
$H11_{eq}-C2$	−177	$H12'_{eq}-C2'$	167	*s*	*s*	*m*	*s*	
$H12_{ax}-C2$	69	$H11'_{ax}-C2'$	−79	*m*	*w*	*m*	*w*	
$H21_{ax}-C1$	100	$H22'_{ax}-C1'$	−88	*w*	*w*	*m*	*w*	
$H22_{eq}-C1$	−145	$H21'_{eq}-C1'$	−156	*m*	*m*	*m*	*s*	
$H11_{eq}-C12_{ax}$	78	$H12'_{eq}-C21'_{ax}$	−75	*w*	*w*	*m*	*w*	
$H11_{eq}-C21_{eq}$	−32	$H12'_{eq}-C12'_{eq}$	36	*m*	*m*	*m*	*m*	
$H12_{ax}-C12_{ax}$	−168	$H11'_{ax}-C21'_{ax}$	170	*s*	*s*	*s*	*m*	
$H12_{ax}-C21_{eq}$	84	$H11'_{ax}-C12'_{eq}$	−79	*w*	*w*	*m*	*w*	

[a] The degree of coupling is ranked as strong (*s*), medium (*m*) and weak (*w*). With respect to torsion angles the ranking is as follows: 0−14°, 165−180°: *s*; 15−74°, 105−164°: *m*; 75−104°: *w*.

The rate constants referring to the two individual pathways with respect to the mesityl rotation on which δ ⇄ λ exchange can occur must add to the rate constants of the overall process as determined by the analysis of the two-site exchange processes (Table 7). Within the margins of error this is in fact the case for all of the four-site exchange processes in compounds **1**−**4**. The rotational pathways which the mesityl groups take as a coupled pair in each case have been described as *L* and *D* (Figure 7−9). From the corresponding rate constants the probabilities with which these pathways are taken were calculated and are shown in Table 7. Rate constants for temperatures other than the ones listed in Table 7 were determined for two compounds by analysis of the behaviour of solutions of these compounds containing the isomers in nonequilibrium concentrations. These solutions were prepared by dissolving crystals of these compounds at low temperatures (see Figure 10). At certain temperatures during the warming up period (**1**: 221, 232 K; **3**: 212, 224, 235 K) the time dependence of the concentration ratio of the two isomers was measured at T = const. The time dependence of this ratio was evaluated by making use of the solution of the corresponding differential equations (see Supporting Information) which is Equation (1) (k: rate constant [s^{-1}]; t_x: time [s]; K: equilibrium constant; r_0: concentration ratio at t = 0 s; r_x: concentration ratio at $t = x$ s). From these k values at different temperatures $\Delta H^{\neq}$ and $\Delta S^{\neq}$ values, relating to the rate constants pertinent to compounds **1** and **3** were evaluated. From the temperature dependence of the equilibrium constants (Figure 10) the ΔH and ΔS values as shown in Table 1 were obtained.

$$-\frac{1}{(K+1)}\cdot\ln\frac{(r_0+1)\cdot(r_x-K)}{(r_x+1)\cdot(r_0-K)}=k\cdot t_x \qquad (1)$$

NMR Spectroscopic Structure Refinement: In order to transform NOE volume integrals into distances[25] some volume integrals referring to known distances had to be selected. The selection used (Table 8) was based on the inspection of the 2D NOE maps with the selection principle allowing only those volume integrals which were free from disturbance by other peaks to be incorporated. The resulting interproton distances for the major isomer of compound **1** as an example are shown in Table 8. These distances were used to define the distance matrix[29] on the basis of the known solid state structures of the compounds.[8,9] Distance geometry calculations were based on a model with λ conformation and another one with δ conformation in each case. From each of the two distance matrices one hundred conformations were allowed to evolve.

Table 7. Rate constants and activation energies for the δ → λ and λ → δ isomerisation of **1**−**4** as obtained from 2D EXSY data

			^{31}P EXSY			^{1}H EXSY					
	T [K]		k_{Twist} [s^{-1}]	$\Delta G^{\neq}$ [kJ mol^{-1}]	ΔG [kJ mol^{-1}]	k_{Twist}[a] [s^{-1}]	$\Delta G^{\neq}$ [kJ mol^{-1}]	ΔG [kJ mol^{-1}]	k_L[b] [s^{-1}]	k_D[b] [s^{-1}]	P_L/P_D[c]
1	299	δ → λ	2.17	71.2	−3.9	1.80(14)	71.7	−3.7	1.23(9)	0.31(3)	0.8:0.2
		λ → δ	0.45	75.1		0.41(4)	75.4		0.27(2)	0.06(1)	
	305	δ → λ	5.46	70.5	−3.7						
		λ → δ	1.25	74.2							
2	299	δ → λ	7.72	68.1	−4.6	6.10(39)	68.7	−4.7	6.64(16)	0.97(7)	0.9:0.1
		λ → δ	1.18	72.7		0.89(6)	73.4		0.99(2)	0.15(1)	
3	299	δ → λ	1.08	73.0	−4.4	0.70(7)	74.0	−4.4	0.60(6)	0.40(7)	0.6:0.4
		λ → δ	0.18	77.4		0.12(1)	78.4		0.10(1)	0.08(1)	
	301	δ → λ	1.18	73.3	−4.6						
		λ → δ	0.19	77.9							
4	299	δ → λ	1.83	71.6	−2.9	1.41(17)	72.3	−2.8	0.71(6)	0.92(7)	0.4:0.6
		λ → δ	0.58	74.5		0.45(5)	75.1		0.24(3)	0.30(2)	
	301	δ → λ	1.45	72.8	−2.7						
		λ → δ	0.49	75.5							

[a] The kinetic data presented in this column are the average of the corresponding rate constants as obtained by evaluating all EXSY peaks stemming from all the protons which show a two-site exchange excluding the ones of the mesityl groups (see table) which are engaged in a four-site exchange (see text). The numbers in parentheses give the estimated standard deviation in units of the least significant digit in each case. [b] Based on the estimated standard deviations of the rate constants a statistical test (student's test[32]) reveals that the values for k_L and k_D refer to two different distributions about different mean values within a confidence limit > 99.9% for compounds **1**−**3**. This means that there are in fact two different pathways *L* and *D* (Figures 7−9) of strongly coupled mesityl rotations. The estimated standard deviation in units of the least significant digit is given in parentheses. [c] P*L*, P*D* are the probabilities of pathways *L* and *D* (Figures 7−9) as inferred from k_L and k_D for each compound.

The initial restraints with respect to NOE-determined distances were set to an allowed variation of ±5% (major isomer) and ±10% (minor isomer) throughout. For those groups for which individual protons could not be assigned the "pseudoatom approach" was used.[30] Methyl groups, the three protons of which lead to one and the same signal, were modelled by a pseudoatom at the centre of the plane formed by the three hydrogen atoms. With respect to NOE distances, which involve these groups, the upper bounds of the corresponding distance intervals were increased by 1 Å. Phenyl groups which were found to be freely rotating (**1**) were described by replacing the pair of *ortho*-protons as well as the pair of *meta*-protons by corresponding pseudoatoms placed on the C_2 axis of the phenyl groups. The upper bound of NOE distances involving these protons was increased by 1.5 Å to 2.0 Å. Methylene protons (COD coligand for **1**−**4**, ethyl groups for **3**) for which the diastereotopic differentiation was found to be insufficient to resolve individual signals for each proton were modelled by a pseudoatom placed in the middle of these protons. The upper bound for NOE distances involving these protons was increased by 0.5 Å. These distance corrections for pseudoatoms as quoted were checked for their appropriateness by inspection of the starting models. The 2 × 100 conformations obtained by DG refinement were finally allowed to refine in the ESFF force field[16] with no NOE restraints imposed on them. Since many of the DG refined conformations relax into one and the same force field optimised conformation only a small number of different conformations remained from the 100 conformations in the starting set. These remaining conformations were found to be very similar to each other for the major isomer. Larger differences between these conformations occurred only with respect to dihedral angles involving methyl groups or phenyl *ortho* positions as the termini (**1**: phenyl; **3**: ethyl; **4**: OMe). For **2** with its DBP ligand constituent only one conformation remained since there are no rotational groups of this kind in this compounds. Only one type of orientation was found for the mesityl groups in each case. The conformation concerning the $PMes_2$ part of the compounds **1**−**4** was found to be roughly the same in each case (Figure 11). In order to decide whether the λ or the δ form was the one to give rise to the NOE data, the following procedure was adopted. The rms values as given by the DG program package which refer to a weighted sum of squares of different classes of distances[17] were taken as one of these criteria. It was found that for the major isomer these rms values were an order of magnitude smaller for the λ conformation than for the δ conformation, i.e. that the major isomer should be the λ one. The minor isomer must then be the δ one. The rms values obtained by DG runs on the minor isomer confirmed this expectation. The quality of agreement between the NOE distances calculated for the best DG structures and the NOE distances inferred from

Table 8. Comparison of calculated and measured distances of the λ isomer of **1**

No.	Atom	Pair[e]	NOE[a] d [Å]	X-ray[b] λ/δ d [Å]	DG[c] λ d [Å]	FF[d] λ d [Å]	No.	Atom	Pair[e]	NOE[a] d [Å]	X-ray[b] λ/δ d [Å]	DG[c] λ d [Å]	FF[d] λ d [Å]	No.	Atom	Pair[e]	NOE[a] d [Å]	X-ray[b] λ/δ d [Å]	DG[c] λ d [Å]	FF[d] λ d [Å]
1[f]	$H11_{eq}$	$H11_{ax}$	1.78	1.75/1.76	1.76	1.76	22	H3	$H11_{eq}$	2.41	2.52/2.53	2.46	2.38	45	$H31,35_{eq}$	$H21_{ax}$	2.22	2.49/2.44	2.61	2.31
2[f]	$H22_{eq}$	$H21_{ax}$	1.78	1.76/1.77	1.76	1.76	23	H3	$H21_{ax}$	2.29	2.27/3.03	2.32	2.30	46	$H31,35_{eq}$	$H22_{eq}$	2.99	3.24/3.14	1.75	2.82
3	H111	H112	2.07	1.75/1.74	1.77	1.76	24	H3	$H22_{eq}$	2.71	2.70/2.33	2.65	2.64	47	$H31,35_{eq}$	H4	2.32	2.89/2.67	1.83	2.39
4	$H31,35_{eq}$	$H32,34_{eq}$	2.12	2.41/2.41	2.44	2.45	25	H3	HO	2.15	2.24/2.81	2.51	2.84	48	$H31,35_{eq}$	H5	2.86	2.84/3.09	1.93	3.28
5	$H37,41_{ax}$	$H38,40_{ax}$	2.24	2.45/2.42	2.47	2.46	26	H3	$H16_{ax}$	3.79	3.86/6.00	3.89	4.03	49	$H31,35_{eq}$	$H18_{ax}$	2.48	2.23/2.15	3.90	2.32
							27	H3	$H20_{ax}$	2.24	2.69/3.97	2.35	2.56	50	$H32,34_{eq}$	H4	4.00	4.33/4.20	4.14	4.34
														51	$H32,34_{eq}$	H5	3.84	3.90/3.98	3.33	4.28
6	$H14_{ax}$	$H18_{ax}$	2.31	2.28/2.18	2.26	2.22	28	$H11_{eq}$	$H20_{ax}$	2.14	2.25/2.23	2.03	2.21	52	$H32,34_{eq}$	$H18_{ax}$	4.01	4.44/4.33	5.33	4.32
7	$H14_{ax}$	$H19_{ax}$	2.51	2.42/2.51	2.43	2.46	29	$H21_{ax}$	$H14_{ax}$	4.01	4.01/4.11	3.91	3.96	53	$H37,41_{ax}$	$H11_{ax}$	2.92	3.18/3.12	2.47	2.60
8	$H16_{ax}$	$H19_{ax}$	2.51	2.51/2.46	2.51	2.50	30	$H21_{ax}$	$H18_{ax}$	2.68	2.47/2.51	2.39	2.50	54	$H37,41_{ax}$	$H22_{eq}$	2.22	2.35/2.30	2.67	2.46
9	$H16_{ax}$	$H20_{ax}$	2.33	2.34/2.38	2.30	2.33								55	$H37,41_{ax}$	HO	3.07	3.69/5.04	4.17	2.86
10	$H23_{eq}$	$H27_{eq}$	2.23	2.40/2.35	2.40	2.30	31	H4	H101	3.28	3.63/3.66	3.43	3.40	56	$H37,41_{ax}$	H4	2.42	2.64/2.75	2.64	2.96
11	$H23_{eq}$	$H28_{eq}$	2.45	2.50/2.49	2.50	2.49	32	H5	$H18_{ax}$	2.90	2.96/3.04	3.04	2.88	57	$H37,41_{ax}$	H5	4.56	4.50/4.57	4.88	4.77
12	$H25_{eq}$	$H28_{eq}$	2.48	2.62/2.44	2.61	2.46	33	H5	H112	3.24	3.64/3.58	3.54	3.68	58	$H37,41_{ax}$	H9	3.59	3.62/3.71	3.42	3.74
13	$H25_{eq}$	$H29_{eq}$	2.23	2.33/2.44	2.30	2.28	34	H8	$H18_{ax}$	2.56	2.59/2.50	2.56	2.54	59	$H37,41_{ax}$	$H29_{eq}$	2.27	2.55/2.45	2.25	2.41
							35	H8	$H23_{eq}$	4.39	4.52/4.46	4.27	4.42	60	$H37,41_{ax}$	H102	4.64	3.95/4.10	4.30	4.38
							36	H8	$H27_{eq}$	2.22	2.21/2.12	2.48	2.25	61	$H37,41_{ax}$	H111	2.53	2.85/2.69	3.37	3.63
14	H4	H111	2.32	2.39/2.26	2.27	2.32	37	H9	$H23_{eq}$	4.67	4.82/4.85	4.82	4.83	62	$H38,40_{ax}$	H4	3.80	4.42/4.58	4.23	4.72
15	H4	H112	2.74	2.88/2.72	2.89	2.88	38	H9	$H25_{eq}$	3.72	4.13/4.15	3.88	4.00	63	$H38,40_{ax}$	$H29_{eq}$	3.40	3.97/3.94	3.74	3.90
16	H5	H61	2.23	2.23/2.23	2.09	2.29	39	H9	$H27_{eq}$	3.21	3.83/3.89	4.18	4.06	64	$H38,40_{ax}$	H111	3.57	3.95/3.98	4.24	4.93
17	H5	H62	2.79	2.47/2.56	2.61	2.53	40	H9	$H29_{eq}$	2.35	2.50/2.53	2.68	2.54					X-ray	DG	FF
18	H8	H71	2.38	2.23/2.29	2.23	2.32	41	H9	H72	3.26	3.58/3.56	3.55	3.65			rms[g]	[Å]	λ/δ	λ	λ
19	H8	H72	2.36	2.78/2.81	2.65	2.87	42	H9	H112	3.65	4.00/4.01	4.12	3.98			1−64		0.29/0.52	0.45	0.36
20	H9	H101	2.35	2.25/2.20	2.26	2.31	43	$H16_{ax}$	$H27_{eq}$	3.57	3.94/3.77	3.83	3.83			1−5		0.22/0.21	0.22	0.23
21	H9	H102	2.71	2.48/2.51	2.61	2.50	44	$H18_{ax}$	H71	2.68	3.20/2.96	3.03	3.11			6−21		0.17/0.16	0.13	0.16
																22−64		0.33/0.62	0.53	0.42
																22−27		0.20/1.23	0.16	0.33

[a] Distances as inferred from NOE measurements. [b] Distances referring to the λ isomer (correct) and those referring to the δ isomer (wrong!) in the solid state structure are given in that sequence separated by a slash. [c] Distances referring to the optimal model from DG refinement. [d] Distances referring to the optimal model from force field refinement. [e] The designators refer to Figures 3 and 4. [f] Contacts used as reference distances. [g] Root mean square (rms) deviations between distances obtained from NOE experiments and distances derived from model structures for selected sets of contacts.

measurement is shown as column DG in Table 8 for the λ isomer of **1**, which is the major isomer in this case as in the cases of **2**−**4**. This is shown in Table 8 for all of the 64 NOE contacts that could be measured for **1**-λ including those contacts that are fixed by the covalent framework. Contacts that may serve as reference contacts have the numbers 1−5 in Table 8. Contacts No. 1 and 2 were used in the transformation of NOE integrals into distances. The rms value relating to all NOE distances is 0.45 Å, the one relating to the potential reference distances is 0.22 Å as shown in Table 8. Distances No. 6−21 (Table 8) refer to 1−3 or 1−4 contacts which are, while being comparatively well fixed by the covalent framework, subject to variation on torsion angles and are therefore not so well suited as reference distances. The rms value for this group of distances is only 0.13 Å. For the comparison of distances involving methyl groups out of the three protons of such a group the one was chosen which had the shortest contact. This principle was also applied to make the proper choice between the two *ortho*- and *meta*-protons of the phenyl groups (Table 8). Contacts No. 22−64 will respond to the conformation, to a larger or lesser extent, due to the fact that there are quite a number of "long" distances above 3.5 Å which, by the nature of the experiment, are less well determined. The agreement is somewhat lower for this set of distances and is found to amount to an rms value of 0.53 Å. When the same type of comparison is made for the structural models derived by force field methods (column FF, Table 8) or from X-ray analysis of the λ isomer (column X-ray, Table 8) the overall agreement is good (Table 8 and rms values given in this table). This means that the average structure in solution is very close to the force field calculated minimum structure that is again very close to the structure determined by X-ray methods in the solid state. When the distances determined for the major isomer are compared with the ones calculated for the δ conformation (known from X-ray structure analysis) the agreement is worse for those classes of distances which contain distances that respond to conformational changes (of course not different for covalently fixed distances), i.e. for the group of all distances No. 1−64 and for the group of distances No. 22−64 (Table 8).

The most discriminating distances are found to be the ones radiating from H3 (Figure 3) as expected. The rms values based on this subset of distances (No. 22−27, Table 8), as calculated by comparison with the λ conformer and the δ conformer of the X-ray structure, are given in Table 8 and show that there can be no doubt about the fact that it is the λ form which corresponds to the conformation of the major isomer.

When the minor isomer of **1** is treated in the same way this same type of rms value is again maximally discriminating. It is found to be 0.31 Å for the correct assignment (δ) and 0.76 Å for the incorrect one (λ) (Table 9). This means that, even though, due to its low concentration, the NOE data for the minor isomer are less accurate and smaller in number, it is possible to discriminate between the two forms for the minor isomer. The same procedure, as explicitly described for **1**, was applied to compounds **2**−**4** leading to the result that, beyond doubt, the major isomer corresponds to the λ conformation in each case. The rms values with respect to the contacts radiating from H3 and referring to the differences between these distances as inferred from NOE measurements and the distances calculated either for the λ or the δ conformer of the X-ray structure, are collected in Table 9.[31] It is seen that these rms values are significantly different for the two assignments in all cases. The correct assignment is the one where the δ conformation is the one corresponding to the minor isomer and the λ conformation corresponds to the average structure of the major isomer. The agreement between the rms values as calculated on the basis of structural models derived from X-ray data or from DG refinement or also from force field refinement (Table 9 ROWSEP="YES") is found to be equally good for **2**−**4** as already observed for **1**.

Table 9. Discrimination between λ and δ isomers on the basis of rms values

[a]	No. of contacts	Major X-ray λ/δ	(λ) DG λ	FF λ	No. of contacts	Minor X-ray δ/λ	(δ) DG δ	FF δ
1	64	0.29/0.52	0.45	0.36	19	0.35/0.46	0.37	0.35
	6	0.20/1.23	0.16	0.33	3	0.31/0.76	0.25	0.33
2	73	0.39/0.75	0.38	0.36	14	0.39/0.41	0.33	0.36
	7	0.25/0.87	0.25	0.22	2	0.20/0.59	0.11	0.16
3	70	0.72/0.77	0.50	0.55	21	0.61/0.74	0.38	0.89
	6	0.10/1.04	0.14	0.09	5	0.22/0.79	0.05	0.37
4	60	0.36/0.50	0.33	0.44	27	0.25/0.30	0.17	0.36
	7	0.52/1.28	0.47	0.44	3	0.24/0.41	0.13	0.19

[a] Column headers have the same meaning as given in the footnote of Table 8. The first line refers to the corresponding rms values as calculated for the total of all the NOE contacts measured in this case, the second line refers only to those contacts which radiate from H3 in each case.

Acknowledgments

We are indebted to the German Science Foundation, SFB 247, HU 151/24-1, /29-1 and the Fonds der Chemischen Industrie for financial support. We are grateful to Prof. H. Friebolin for helpful discussions.

[1] [1a] M. Nógradi, *Stereoselective Synthesis*, 2nd ed., VCH, Weinheim, **1995**. [1b] H. Brunner, W. Zettlmeier, *Handbook of Enantioselective Catalysis with Transition Metal Compounds*, VCH, Weinheim, **1993**.

[2] [2a] B. D. Vineyard, W. S. Knowles, M. J. Sabacky, G. L. Bachmann, D. J. Weinkauff, *J. Am. Chem. Soc.* **1977**, *99*, 5946−5952. [2b] W. S. Knowles, M. J. Sabacky, B. D. Vineyard, D. J. Weinkauff, *J. Am. Chem. Soc.* **1975**, *97*, 2567−2568.

[3] [3a] J. M. Brown, D. Parker, *J. Chem. Soc., Chem. Commun.* **1980**, 342−344. [3b] W. C. Christopfel, B. D. Vineyard, *J. Am. Chem. Soc.* **1979**, *101*, 4406−4408.

[4] [4a] R. Noyori, M. Ohta, Y. Hsiao, M. Kitamura, T. Ohta, H. Takaya, *J. Am. Chem. Soc.* **1986**, *108*, 7117−7119. [4b] M. Kitamura, M. Tokunaga, R. Noyori, *J. Org. Chem.* **1992**, *57*, 4053−4054. [4c] B. Heiser, E. A. Broger, Y. Crameri, *Tetrahedron: Asymmetry* **1991**, *2*, 51−62.

[5] [5a] J. Sprinz, G. Helmchen, *Tetrahedron Lett.* **1993**, *34*, 1769−1772. [5b] P. von Matt, A. Pfaltz, *Angew. Chem.* **1993**, *105*, 614−615; *Angew. Chem. Int. Ed. Engl.* **1993**, *32*, 566−567. [5c] G. J. Dawson, C. G. Frost, J. M. J. Williams, S. J. Coote, *Tetrahedron Lett.* **1993**, *34*, 3149−3150. [5d] J. Sprinz, M. Kiefer, G. Helmchen, M. Reggelin, G. Huttner, O. Walter, L. Zsolnai, *Tetrahedron Lett.* **1994**, *35*, 1523−1526.

[6] [6a] J. D. Dunitz, J. Waser, *J. Am. Chem. Soc.* **1972**, *94*, 5645−5650. [6b] J. D. Dunitz, *Tetrahedron* **1972**, *28*, 5459−5467.

[7] [7a] P. A. McNeil, N. K. Roberts, B. Bosnich, *J. Am. Chem. Soc.* **1981**, *103*, 2273−2280. [7b] J. Bakos, I. Tóth, B. Heil, G. Szalontai, L. Párkányi, V. Fülöp, *J. Organomet. Chem.* **1989**, *370*, 263−276.

[8] J. Karas, G. Huttner, K. Heinze, P. Rutsch, L. Zsolnai, *Eur. J. Inorg. Chem.* **1999**, 405−420.

[9] CCDC-148008 (**3**) and -148009 (**7**) contain the supplementary crystallographic data for this paper. These data can be obtained free of charge at www.ccdc.cam.ac.uk/conts/retrieving.html or from the Cambridge Crystallographic Data Centre, 12, Union Road, Cambridge CB2 1EZ, UK [Fax: (internat.) + 44-1223/336-033; E-mail: deposit@ccdc.cam.ac.uk].

[10] A. Bax, M. F. Summers, *J. Am. Chem. Soc.* **1986**, *108*, 2093−2094.

[11] [11a] G. Bodenhausen, D. J. Ruben, *Chem. Phys. Lett.* **1980**, *69*, 185−188. [11b] L. E. Kay, P. Keifer, T. Saarinen, *J. Am. Chem. Soc.* **1992**, *114*, 10663−10665. [11c] A. G. Palmer III, J. Cavanagh, P. E. Wright, M. Rance, *J. Magn. Reson.* **1991**, *93*, 151−170. [11d] J. Schleucher, M. Schwendinger, M. Sattler, P. Schmidt, O. Schedletzky, S. J. Glaser, O. W. Sørensen, C. Griesinger, *J. Biomol. NMR* **1994**, *4*, 301−306.

[12] [12a] U. Piantini, O. W. Sørensen, R. R. Ernst, *J. Am. Chem. Soc.* **1982**, *104*, 6800−6801. [12b] M. Rance, O. W. Sørensen, G. Bodenhausen, G. Wagner, R. R. Ernst, K. Wüthrich, *Biochem. Biophys. Res. Commun.* **1983**, *117*, 479−485.

[13] J. Jeener, B. H. Meier, P. Bachmann, R. R. Ernst, *J. Chem. Phys.* **1979**, *71*, 4546−4563.

[14] [14a] D. A. V. Morton, A. G. Orpen, *J. Chem. Soc., Dalton Trans.* **1992**, *4*, 641−653. [14b] K. Mislow, *Acc. Chem. Res.* **1976**, *9*, 26−33. [14c] H. B. Bürgi, *Acc. Chem. Res.* **1983**, *16*, 153−161. [14d] H. B. Bürgi, *Acta Crystallogr., Sect. B* **1988**, *44*, 445−448. [14e] S. Beyreuther, J. Hunger, G. Huttner, S. Mann, L. Zsolnai, *Chem. Ber.* **1996**, *129*, 745−757. [14f] S. Beyreuther, A. Frick, J. Hunger, G. Huttner, B. Antelmann, P. Schober, R. Soltek, *Eur. J. Inorg. Chem.* **2000**, 597−615.

[15] In the original paper[8] the sense of chirality for **2** was erroneously assigned as (*S*).

[16] [16a] *Discover User Guide*, versions 2.9.7 & 95.0/3.00, Biosym/MSI, **1995**. [16b] S. Barlow, A. L. Rohl, S. Shi, C. M. Freeman, D. O'Hare, *J. Am. Chem. Soc.* **1996**, *118*, 7578−7592. [16c] N. Jäger, U. Schilde, *Struct. Chem.* **1998**, *9*, 77−93.

[17] *NMRchitect 98.0, DGII* program package, Molecular Simulations, Inc., 9685 Scranton Road, San Diego, CA 92121, **1998**.

[18] [18a] K. Wüthrich, *Science* **1989**, *243*, 45−50. [18b] K. Wüthrich, *Methods Enzymol.* **1989**, *177B*, 125−131. [18c] T. F. Havel, *Prog. Biophys. Mol. Biol.* **1991**, *45*, 43−78. [18d] M. P. Williamson, J. P. Waltho, *Chem. Soc. Rev.* **1992**, *21*, 227−236. [18e] J. M. Blaney, J. S. Dixon in *Reviews in Computational Chemistry*, vol. 5 (Eds.: K. P. Lipkowitz, D. B. Boyd), VCH Publishers, Inc., New York, **1996**, chapter 6.

[19] U. Burkert, N. L. Allinger, *Molecular Mechanics*, ACS monograph, Washington, **1989**.
[20] [20a] G. Binsch, *Top. Stereochem.* **1968**, *3*, 97−192. [20b] R. Bucourt, *Top. Stereochem.* **1974**, *8*, 159−224. [20c] G. M. Kellie, F. G. Riddell, *Top. Stereochem.* **1974**, *8*, 225−269.
[21] [21a] J. Halpern, D. P. Riley, A. S. C. Chan, J. J. Pluth, *J. Am. Chem. Soc.* **1977**, *99*, 8055−8057. [21b] A. S. C. Chan, J. Halpern, *J. Am. Chem. Soc.* **1980**, *102*, 838−840. [21c] P. S. Chua, N. K. Roberts, B. Bosnich, S. J. Okrasinski, J. Halpern, *J. Chem. Soc., Chem. Commun.* **1981**, 1278−1280. [21d] J. M. Brown, P. A. Chaloner, *Tetrahedron Lett.* **1978**, *21*, 1877−1880. [21e] C. R. Landis, J. Halpern, *J. Am. Chem. Soc.* **1987**, *109*, 1746−1754.
[22] A paper describing the force field model that precisely predicts the observed behaviour is published aside: V. Schulz, A. Frick, G. Huttner, *Eur. J. Inorg. Chem.* **2002**, 3111−3128, preceding paper.
[23] [23a] E. W. Hansen, *Anal. Chem.* **1985**, *57*, 2993−2994. [23b] A. L. Van Geet, *Anal. Chem.* **1970**, *42*, 679−680.
[24] *FELIX 98.0*, NMR processing package, Molecular Simulations, Inc., 9685 Scranton Road, San Diego, CA 92121, **1998**.
[25] B. A. Borgias, M. Gachin, D. Kerwood, T. L. James, *Progr. NMR Spectrosc.* **1990**, *22*, 83−100.
[26] C. L. Perrin, T. J. Dwyer, *Chem. Rev.* **1990**, *90*, 935−967.
[27] [27a] C. L. Perrin, R. K. Gipe, *J. Am. Chem. Soc.* **1984**, *106*, 4036−4038. [27b] R. Willem, M. Biesemans, K. Hallenga, G. Lippens, F. Malaisse-Lagae, W. J. Malaisse, *J. Biol. Chem.* **1992**, *267*, 210−217. [27c] R. Willem, *Prog. NMR Spectrosc.* **1987**, *20*, 1−94.
[28] Mathematica 4.0: S. Wolfram, *The Mathematica Book*, 3rd ed., Wolfram Media/Cambridge University Press, Cambridge, **1996**.
[29] [29a] G. M. Crippen, T. F. Havel, *Distance Geometry and Molecular Conformation*, Research Studies Press, Ltd., Somerset, England, **1988**. [29b]G. M. Crippen, *J. Comp. Phys.* **1977**, *24*, 96−107. [29c] G. M. Crippen, T. F. Havel, *Acta Crystallogr., Sect. A* **1978**, *34*, 282−284. [29d] I. D. Kuntz, J. F. Thomason, C. M. Oshiro, *Methods Enzymol.* **1989**, *177B*, 159−204. [29e] D. F. Mierke, M. Reggelin, *J. Org. Chem.* **1992**, *57*, 6365−6367. [29f] M. Reggelin, M. Köck, K. Conde-Frieboes, D. F. Mierke, *Angew. Chem.* **1994**, *106*, 822−824; *Angew. Chem. Int. Ed. Engl.* **1994**, *33*, 753−755. [29g] M. Köck, J. Junker, *J. Org. Chem.* **1997**, *62*, 8614−8615.
[30] M. Reggelin, H. Hoffmann, M. Köck, D. F. Mierke, *J. Am. Chem. Soc.* **1992**, *114*, 3272−3277.
[31] In the case of **2**, where only one twist conformation was observed in the crystal, the opposite one was constructed by inverting the structure and exchanging the positions of H3 and HO at the central carbon atom of the ligand.
[32] R. Zurmühl, *Praktische Mathematik*, 5th ed., Springer-Verlag, Berlin, Heidelberg, **1965**.

Received November 12, 2001
(publication delayed on the authors' request)
[I01452]